Prepared for submission to SPSC

NA64 Status Report 2026

The NA64 Collaboration[1]

Abstract: NA64 is a fixed-target experiment at the CERN SPS searching for dark-sector particles and other physics beyond the Standard Model using missing-energy and missing-momentum techniques with electron, positron, muon and hadron beams. In this report, we present the latest results of the experiment and summarize the status of the analyses of the data collected before LS3. The electron programme has accumulated an enlarged data sample and demonstrated improved suppression and control of the dominant backgrounds, while the positron programme exploits resonant annihilation to extend the sensitivity to light dark matter. The muon programme has completed the first unblinding of the 2023 data, probing new parameter space for dark sectors coupled predominantly to second-generation leptons, while the hadron programme is developing complementary searches for dark sectors coupled to quarks. We also report on the successful 2025–2026 data-taking campaigns and on detector and beam studies aimed at operation at higher intensities. Finally, we present the planned upgrades and physics programme during LS3 and Run 4, which will allow NA64 to probe most of the remaining parameter space for canonical thermal light dark matter scenarios and a broad range of other well-motivated dark-sector models.

CERN-SPSC-2026-022 / SPSC-SR-384
25/08/2026

[1] http://na64.web.cern.ch/

Contents

1 Introduction **2**

2 Status of NA64 **3**

2.1 NA64e^- at H4 beamline 3

2.1.1 Latest results for an invisibly-decaying $B-L$ Z' 3

2.1.2 Latest results for ALPs 3

2.1.3 Status of the 2024-2025 $A' \rightarrow$ invisible analysis 4

2.1.4 Summary of the 2026 run 10

2.2 NA64e^+ at H4 beamline 12

2.3 NA64 hadron 13

2.3.1 First proof-of-concept K^0_S, K^0_L results 13

2.3.2 CEX cross sections and results from 2025 run 14

2.4 NA64μ at M2 beamline 17

3 NA64 plans during LS3 and Run 4 **21**

3.1 Planned physics analysis during LS3 period 21

3.2 Detector upgrade, tests and measurements during LS3 23

3.2.1 NA64$e^{-/+}$ 23

3.2.2 NA64μ 25

3.2.3 NA64h 26

3.3 Physics goals for Run 4 and measurements foreseen at PS/SPS during LS3 26

3.3.1 Plan of measurements at PS during LS3 27

3.3.2 Plan of measurements at SPS after LS3 28

4 Summary **28**

5 Publications **32**

1 Introduction

NA64 pioneered the active dump/missing energy technique in the quest for dark sectors at the CERN SPS. Using this approach (see Fig.1), the current NA64 research program addresses three key and complementary directions in dark-sector physics that can be explored at the SPS:

(i) world-leading search for Light Dark Matter (LDM) and other BSM physics with masses below the electroweak scale ($\ll 100$ GeV) combining the results from electron and positron beams at H4;

(ii) search for dark sectors predominantly coupled to the second lepton generation and light dark matter with the M2 muon beam;

(iii) search for leptophobic dark sectors predominantly coupled to light SM quarks with the SPS hadronic beams.

Recently, using data collected at the H4 beamline, NA64 set the most stringent upper limits on the kinetic-mixing parameter ϵ for dark-photon (A') masses below 350 MeV. These results also constrain scalar and Majorana light dark matter models with $\alpha_D \leq 0.1$ and $m_{A'} > 3m_\chi$ over the mass range $1 \leq m_\chi \leq 100$ MeV. The results based on the data collected between 2016 and 2022 were published in Phys. Rev. Lett. [1] and selected as an Editors' Suggestion.

In this report, we present the latest results from the NA64 programme using electron, positron, muon, and hadron beams. We also provide an update on the ongoing analyses of the data collected at H4 and M2 and discuss the experiment's future prospects after LS3.

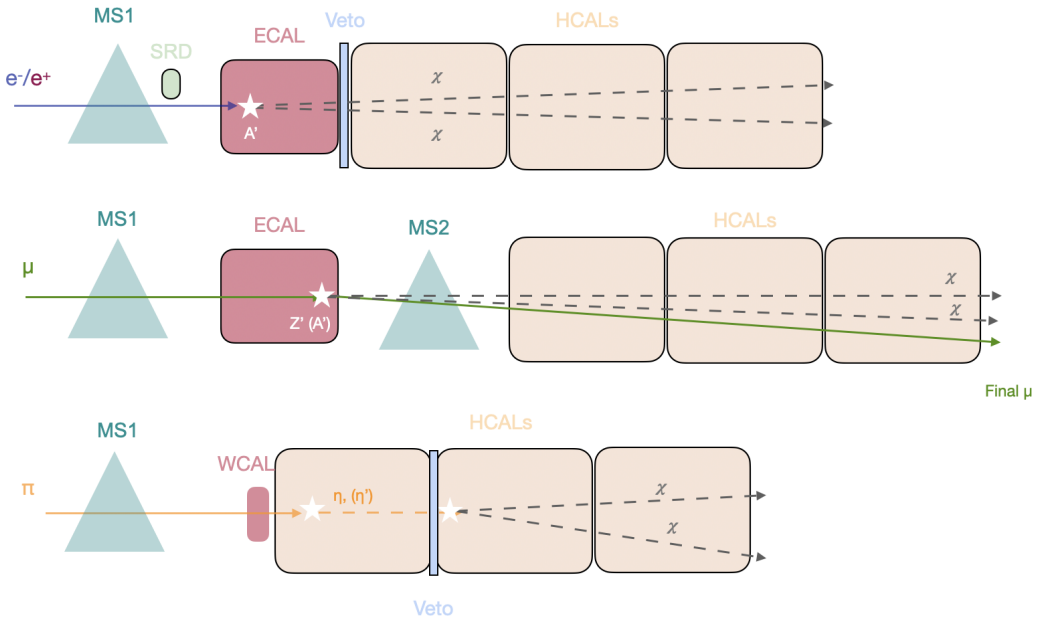

Figure 1. Schematics of the missing energy/momentum technique used by NA64 combining initial e^-, e^+, μ and π beams

2 Status of NA64

2.1 NA64e^- at H4 beamline

2.1.1 Latest results for an invisibly-decaying $B-L$ Z'

Extensions of the Standard Model featuring an additional $U(1)_{B-L}$ gauge symmetry provide a compelling framework linking the origin of neutrino masses to possible dark matter candidates. The associated gauge boson, Z', couples directly to Standard Model fermions and can be produced in fixed-target experiments through electron-nucleus interactions. In Fig. 2, we present constraints on the coupling constant g_{B-L} obtained using the full electron-beam dataset collected between 2016 and 2022, corresponding to $(9.4 \pm 0.5) \times 10^{11}$ electrons on target. The analysis includes the resonant e^+e^- annihilation production channel, which enhances sensitivity in the mass range $m_{Z'} \in [200, 300]$ MeV. For the unbroken $U(1)_{B-L}$ case, our limits exceed those from dedicated neutrino-scattering experiments, providing the most stringent laboratory bounds on g_{B-L} for sub-GeV masses of the new boson. In scenarios where the Z' couples to dark matter, the decay width is dominated by invisible channels, and the corresponding exclusion limits can be directly derived from the NA64 invisible-mode analysis. The manuscript summarising the results is currently under peer review [2].

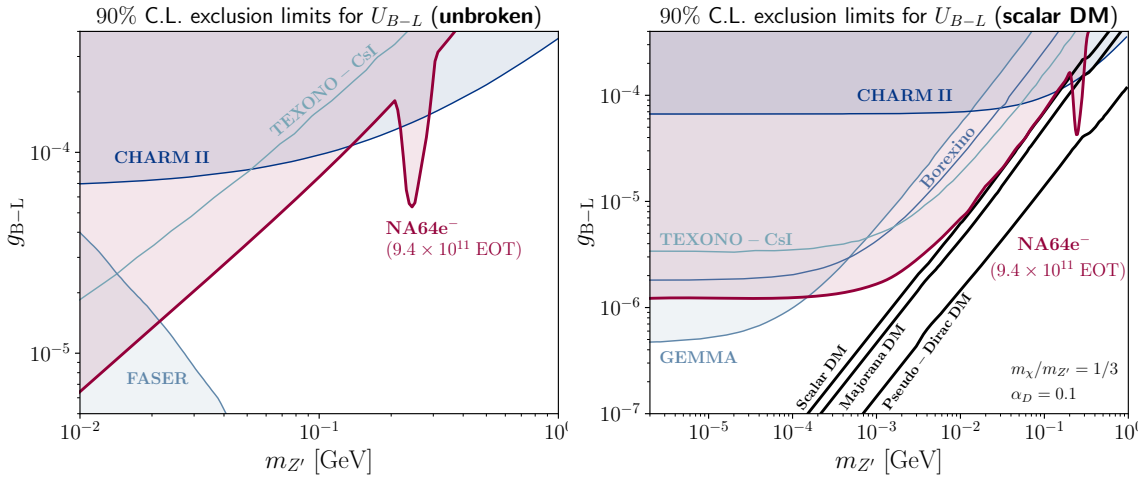

Figure 2. 90% C.L. exclusion limits in the $(m_{Z'}, g_{B-L})$ plane obtained by NA64 for an invisibly decaying $U(1)_{B-L}$ Z' using the combined 2016–2022 dataset in the case of an unbroken $B-L$ symmetry with Dirac neutrinos (top) and a direct coupling with a scalar DM particle (bottom). The DM relic targets have been taken from [3].

2.1.2 Latest results for ALPs

Axion-Like Particles (ALPs) are pseudo-Nambu-Goldstone bosons that serve as dark matter candidates or compelling mediators between the dark and SM sectors. The NA64 experiment is sensitive to both photophilic and electrophilic ALPs produced in electromagnetic

showers, which subsequently decay downstream into photon pairs ($a \to \gamma\gamma$) or electron-positron pairs ($a \to e^+e^-$), either within the downstream HCAL modules or beyond the active detector volume. The former case yields a visible displaced energy signature, whereas the latter is probed via a missing energy signature.

The 2022 and 2023 data-taking periods, corresponding to a combined statistics of 1.03×10^{12} EOT, were analyzed to search for visible signatures in the second and third HCAL modules. The first module serves as a veto to reject target electro- and photo-nuclear interactions that produce leading neutral hadrons, which exhibit a HCAL punch-through probability on the order of 10^{-3}. The signal region was defined using a minimal ECAL missing energy threshold of 40 GeV. A targeted shower-shape selection applied within the HCAL decay volume, designed to isolate collimated electromagnetic showers from broader hadronic showers, provided a further background suppression factor of 10^{-3}–10^{-2} for neutrons and neutral kaons, which constitute the dominant background species. The total background yield from target inelastic interactions was estimated to be 0.21 ± 0.06 events for the 2022 dataset (5.88×10^{11} EOT) and 0.11 ± 0.03 events for the 2023 dataset (4.4×10^{11} EOT).

Following the unblinding of the data, zero candidate events were observed in the signal region, yielding enhanced constraints on the ALP parameter space. Figure 3 shows the resulting exclusion limits for photophilic ALPs derived from the full 2016–2023 dataset (1.31×10^{12} EOT), where the lower boundary in coupling is set by the invisible search constraints recasted from the unblinded 2016–2022 data. These results set new upper limits on the ALP-photon coupling $g_{a\gamma\gamma}$ for ALP masses up to $m_a \approx 77$ MeV. The 2024 dataset visible signature analysis is ongoing, in parallel with the standard invisible one and it is planned to be included in a new publication summarising ALP searches with the 2016-2024 dataset, corresponding to 1.79×10^{12} EOT.

2.1.3 Status of the 2024-2025 $A' \to$ invisible analysis

Status of 2024 data analysis We are in the process of finalizing the reconstruction and the blinded analysis of the data collected during the 2024 run, in which a total of 4.8×10^{11} electrons on target were collected, exploiting an experimental setup analogous to the 2023 one. Specifically, a single VHCAL prototype was installed before the ECAL to suppress backgrounds induced by upstream electro-production interactions of the primary particle with beamline materials (see the top plot of Fig. 8). As in 2023, a pre-scaler was included in the trigger system to save calibration trigger events in parallel with the physics data. In this way, we can constantly monitor the variations in the response of every calorimeter cell throughout data-taking. This information is then included as spill-by-spill and run-by-run corrections to the energies of all calorimeters, complementary to the data acquired with the LED-based light monitoring system. The data reconstruction pipeline was significantly improved by introducing a waveform fit-based algorithm to reconstruct signals from all calorimeter channels and determine the hit time and amplitude, handling pile-up events in which two or more beam particles impinge on the detector almost at the same time, with the corresponding PMT signals partially superimposed within the same readout window. For the ECAL detector, a preliminary version of a multiple-clusters

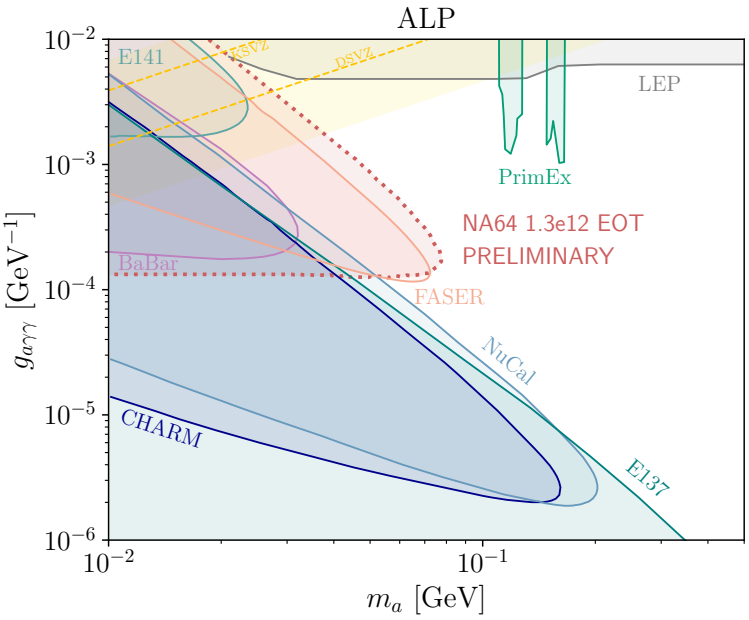

Figure 3. 90% C.L. exclusion limits in the $(m_a, g_{a\gamma\gamma})$ plane obtained by NA64 for visible ALP signatures using the combined 2016–2023 dataset and recasting 2016–2022 invisible A' constraints.

reconstruction algorithm was also implemented. Exploiting time and topological matching between multiple peaks from different cells, the algorithm reconstructs the time and the total deposited energy from different particles impinging on the calorimeter at close times.

To assess the detector stability throughout the whole data-taking and check the dataset normalization and consistency, a detailed analysis of so-called "di-muon" events was performed, in which the impinging electron radiatively produces in the ECAL a $\mu^+\mu^-$ pair through the electromagnetic interaction with the thick-target nuclei (N), according to the reaction $e^-N \to e^-N\mu^+\mu^-$. The upstream signature of these events closely resembles that expected for the LDM signal, consisting of a properly reconstructed 100 GeV/c electron track identified by the synchrotron radiation detector (SRD), in coincidence with a low-energy electromagnetic shower in the ECAL. For this reason, the analysis of these events provides a direct assessment of the detection efficiency and can be used to cross-check the overall normalization. Owing to the specific MIP signature in the VETO and HCAL, di-muon events can be efficiently selected by applying a cut on the deposited energy within each HCAL module - we skimmed the whole dataset selecting events with energy deposition in each HCAL module central cell to be between 1 GeV and 12 GeV, and further cleaned the event sample through the requirement of at least 800 keV deposited in each SRD cell, in order to reject beam-contaminating muons, and with a reconstructed track with momentum between 90 GeV/c and 110 GeV/c. A cut on the total energy deposition in the ECAL, required to be less than 70 GeV, was also introduced to avoid any bias in the dataset due to possible variations of the missing energy trigger threshold during the run.

For each production run, the absolute di-muon rate per electron on target $Y_{\mu\mu}$ was

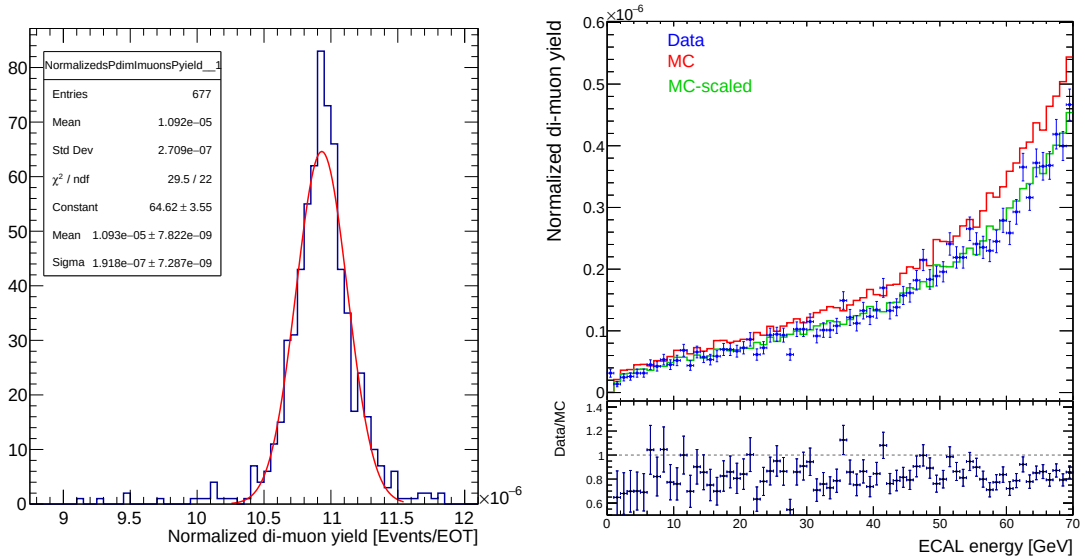

Figure 4. **Left:** efficiency-corrected normalized di-muon yield distribution for all 2024 production runs. **Right:** energy spectrum of di-muon events for an illustrative production run, comparing the experimental result (black) with the Monte Carlo prediction (red). The latter has been scaled by a factor 0.834 (green) to match data normalization. The bottom panel shows the ratio between data and Monte Carlo distributions, before the scaling - see text for further details.

computed dividing the measured event yield $N_{\mu\mu}$, of the order of 8000 events for a complete run, by the efficiency η of the selection cuts and by the number of accumulated EOT, obtained from the counts of the scaler reading the signal after the coincidence of the scintillator counters including the delay issued by the DAQ to inhibit new triggers while the system is processing an event ($SV_{\rm busy}$). The efficiency of the upstream selection cuts – SRD and tracking – was estimated directly from calibration data, exploiting the fact that, at first order, it is the same for all impinging electrons, independently of the interactions eventually occurring downstream. A clean sample of 100 GeV/c impinging e^- was selected by the requirement of an energy deposition in the ECAL between 90 GeV and 110 GeV, and processed through the same analysis chain. The obtained result is shown in Fig. 4, left panel - each entry in the histogram corresponds to a single production run. The average value reads approximately $\overline{Y} = (1.093 \pm 0.001) \times 10^{-5}$, with standard deviation $\sigma_Y = (1.92 \pm 0.07) \times 10^{-7}$. The same procedure, repeated including only runs with at least 190 accumulated spills, results in the average value $(1.094 \pm 0.001) \times 10^{-5}$ and standard deviation $(1.60 \pm 0.08) \times 10^{-7}$. The relative width σ/μ thus reads $(1.46 \pm 0.07)\%$, in reasonable agreement with the statistical fluctuations expected for $N_{\mu\mu}$, confirming the stability of the NA64 experimental apparatus throughout the 2024 electron-beam run.

To assess the dataset normalization, the normalized ECAL energy spectrum for di-muon events was compared with the prediction from Monte Carlo simulations, executed using a realistic description of impinging beam angular and positional distribution, determined from the calibration data. The result for a representative run is shown in Fig. 4,

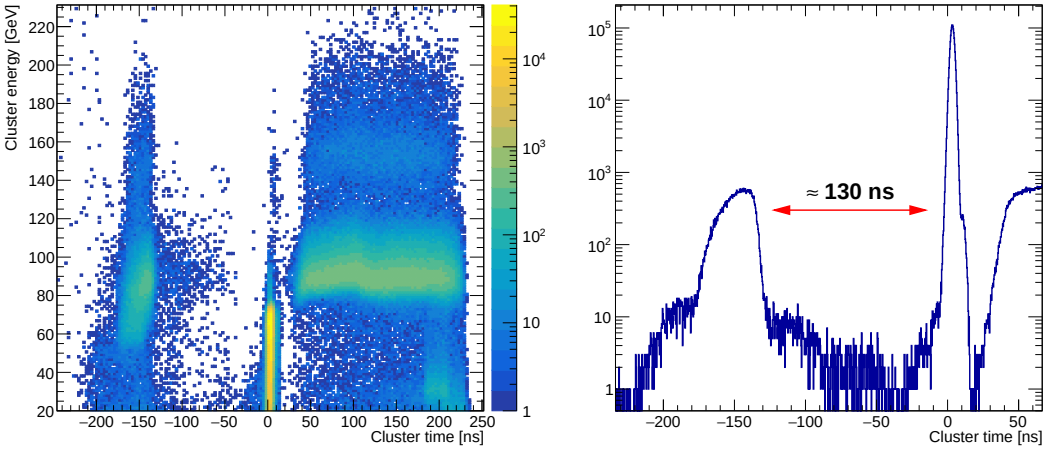

Figure 5. Trigger analysis from the 2024 dataset exploiting di-muon events. **Left:** correlation between cluster energy (vertical axis) and cluster time relative to master time (horizontal axis) for all clusters reconstructed in di-muon events (period-1 data). **Right:** the clusters time distribution, showing the ≈ 130 ns gap due to the missing energy VETO signal in the trigger. See text for further details.

right panel, reporting in black (red) the data (MC) result, as well as their ratio. We observe that the Monte Carlo distribution closely resembles the data, with an overall $\mathcal{F}_{\mu\mu} \approx 0.834$ factor difference for the overall normalization. This discrepancy originates from the finite dead time of the trigger, introduced by the ECAL energy-sum discriminator output used to implement the missing-energy veto condition. The effect can be directly visualized in Fig.5, left panel, showing the correlation between the energy and time of all ECAL clusters reconstructed in di-muon events. Besides the triggered low-energy cluster at $T \approx 0$, corresponding to the di-muon interaction, a clear absence of preceding high-energy clusters is observed. The corresponding cluster-time distribution, shown in the right panel of Fig.5, allows the width of this dead-time window to be measured, yielding $\tau \approx 130$ ns. Since the trigger acceptance depends only on the absence of previous beam particles within this interval, the measured di-muon yield is reduced by a factor $\exp(-R\tau)$, where R is the average beam rate. For the 2024 running conditions ($R \approx 1.35$ MHz), this corresponds to a correction factor of $\exp(-R\tau) \approx 0.84$, in very good agreement with the normalization deficit observed in the simulated and measured di-muon yields. During the 2025 run, this effect has been partially compensated by optimizing the length of the logic signals within the trigger logic - the corresponding analysis is currently in progress.

The whole production dataset was processed to the "standard" NA64 cutflow to search for an invisibly-decaying A'. Since the detector configuration is unchanged with respect to the previous data-taking campaign, in the first iteration the same selection criteria were applied. Events were filtered requiring a well-reconstructed impinging track with momentum in the range [90-110] GeV/c, in-time with a sizable signal in the synchrotron radiation detector and with no energy deposition in the downstream veto and hadronic calorimeters. Furthermore, a cut on the transverse shape of the electromagnetic shower

measured by the ECAL was introduced, exploiting the χ^2_{shower} observable. This is defined as the sum over all calorimeter cells of the squared difference between the deposited energy fraction and that expected from a pure electromagnetic signal, divided by the corresponding expected width squared:

$$\chi^2_{shower} = \sum_i \frac{(E^i_{dep} - E^i_{exp})^2}{\sigma_i^2} \quad , \tag{2.1}$$

where all quantities are normalized to the nominal 100 GeV beam energy. The quantities E^i_{exp} and σ_i are evaluated directly from the data, exploiting events collected during minimum-bias calibration runs. The result is shown in Fig. 6, with the signal region defined by the two conditions $E_{ECAL} < 60$ GeV and $E_{HCAL} < 1$ GeV still blinded. The efficiency of the selection cuts, evaluated on a sample of 100 GeV/c impinging electron events from the calibration dataset, is approximately 0.5, dominated by tracking effects.

While the final optimization of signal selection criteria and final signal box definition is currently in progress, here we describe a possible optimization strategy of the χ^2_{shower} cut, aimed at reducing the background yield in the sideband region. As shown in Fig. 6, some events, surviving the cutflow, accumulate close to the blinded region, ($E_{ECAL} \simeq$ 60 GeV); these, consisting of high-transverse-momentum hadrons produced via electron-nuclear interactions upstream of the target, can be rejected by optimizing the χ^2_{shower} cut, which is particularly sensitive to an energy deposition in the different ECAL cells not compatible with a "clean" electromagnetic shower, as expected for the signal. The χ^2_{shower} cut is usually defined with a data-driven procedure, exploiting the signal prompt provided by the di-muons events sample collected during the data taking (see previous paragraphs). As shown in the blue histogram in Fig. 7, left panel, representing the χ^2_{shower} distribution of the di-muons sample, the spectra for signal-like events is sharply peaked at $\chi^2_{shower} \simeq 0.7$, rapidly decreasing for $\chi^2_{shower} > 1$. In contrast, the red histogram shows the same distribution for the sideband events close to the blinded region, i.e. all the events surviving the cutflow and satisfying the condition $E_{ECAL} < 70$ GeV and $E_{HCAL} < 5$ GeV. These feature significantly larger χ^2_{shower} values if compared to the signal prompt, which can be exploited to reject them. As an example, if one sets a cut value so to get an 85% signal efficiency, as shown by the green dashed line in Fig. 7, most of the sideband events are rejected, resulting in a significantly improved background projection in the signal region. Indeed, the different nature of the sideband events with respect to signal-like events appears evident in the right panel of Fig. 7, showing, in the same 2D plot, the χ^2_{shower} versus the ECAL energy distribution for di-muon events and the sideband events surviving the cutflow (red triangles).

Status of 2025 data analysis Similar to the 2023-2024 runs, the 2025 run aimed at increasing our electrons-on-target statistics in the search for A' invisible decay, as well as to study the improvement in the level of the detector hermeticity and background rejection by installing an additional, second VHCAL module identical to the one used in 2023/2024 runs and compare the results with Monte Carlo predictions (see also Fig. 8).

A preliminary analysis of a fraction of the dataset was presented in last year's SPSC report. Since then, substantial progress has been made in the data processing and recon-

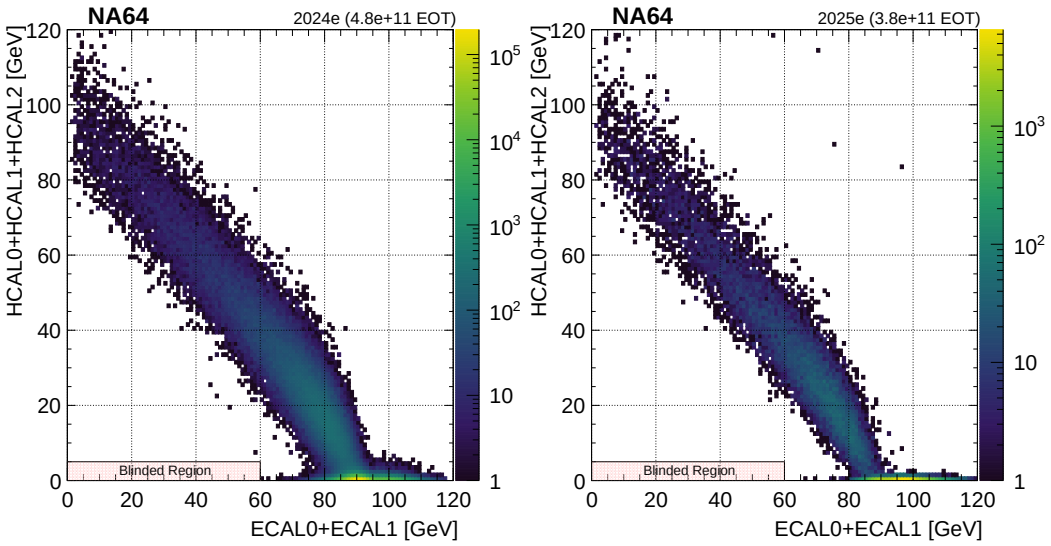

Figure 6. Distribution of events in the (EECAL; EHCAL) plane for 2024 (4.8×10^{11} EOT) and 2025 (3.8×10^{11} EOT) datasets. The two pink boxes show the blinding region.

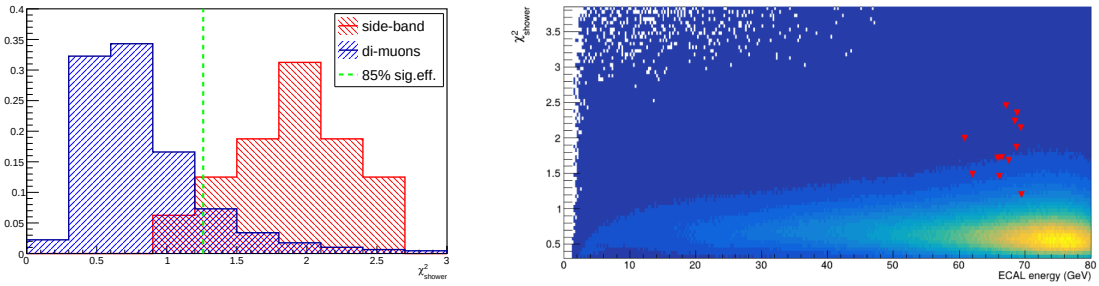

Figure 7. **Left:** the blue histogram shows the χ^2_{shower} distribution of the signal prompt (di-muon events sample), while the red histogram shows the distribution for the side-band background events. See the text for more details. **Right:** the histogram shows the χ^2_{shower} VS ECAL energy distribution for di-muon events; the red triangles indicate the sideband events surviving the cutflow.

struction chain, including the implementation of an optimized tracking algorithm and a fit-based waveform reconstruction procedure. The latter development fully exploits the improved signal quality provided by the new "Waveboard" digitizers, which were used to read out all calorimeter channels during the 2025 run.

The whole dataset has already been processed with an almost final version of calibration constants, including run-by-run and spill-by-spill corrections to each channel response. The data analysis is currently in progress. The event selection criteria closely follow the strategy established for the 2024 dataset, with two key modifications reflecting detector upgrades. First, a threshold of 1.5 GeV is applied to each of the two VHCAL modules. Second, the SRD cut was revised to exploit the upgraded LYSO crystal array, replacing the former copper-scintillator shashlik calorimeter. The new selection requires multiple hit crystals with a total integrated energy deposition constrained between 7.5 MeV and

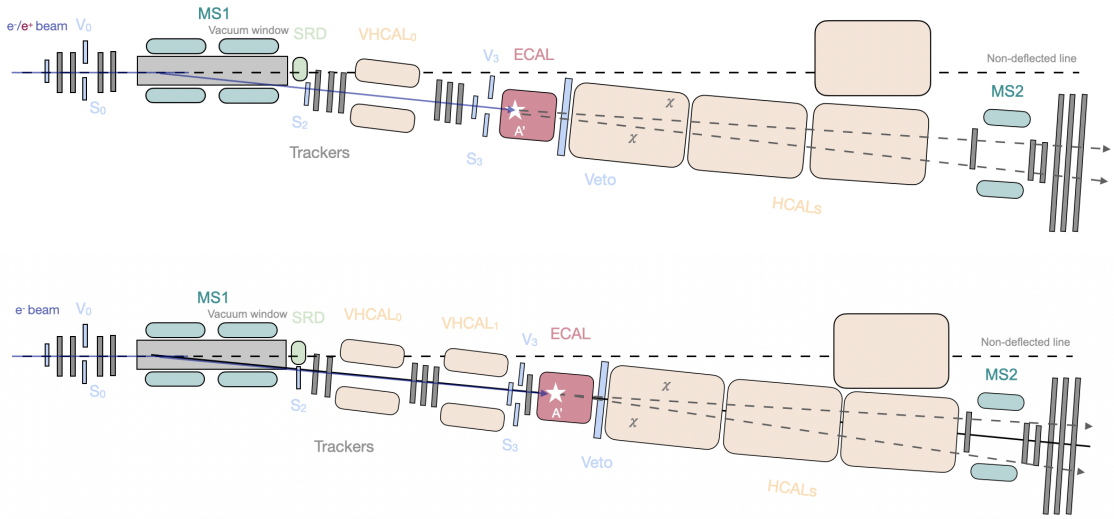

Figure 8. Schematic illustration of the NA64 setup used in 2023/2024 runs (top plot) and in 2025 (bottom plot) to search for the $A' \rightarrow$ invisible decay at H4.

250 MeV. In Fig. 6, right panel, we show the current result in terms of distribution of surviving events in the (EECAL; EHCAL) plane - the corresponding efficiency, evaluated as in 2024, is approximately 0.38, with a $\simeq$ 20% reduction with respect to 2024 due to an increased extend of beam-instability periods observed throughout the run, in which the performances of the tracking system are reduced.

Background projections comparison between 2024 and 2025 Following the introduction of the second VHCAL module in 2025, a substantial reduction in the resulting background from high-p_t hadrons originating from upstream interactions with the beam material was achieved. Fig. 9 shows an order-of-magnitude improvement in the suppression of the tails, resulting from the increased hermeticity of the two-VHCAL setup and refined arrangement of the material along the beamline consistent with the prediction of our detailed MC study [4].

2.1.4 Summary of the 2026 run

In 2026, the SPSC granted us 54 days of data-taking from March 11th until May 4th. For the first time, NA64 was the first user of the beamline, allowing us to reduce the time dedicated to installation, commissioning, and calibration by one week. In addition, for the first time we requested two weeks prior our run at PS to prepare the DAQ system and test the new unmultiplexed Micromegas detector produced for this run (further details about the detector performance are given in the later sections). The setup was the same as the one used in 2025, as the main goal of the run was to increase the statistics with the two-VHCAL configuration to achieve $\sim 10^{12}$ EOT (see a sketch in Fig. 8). We started data-taking on 20th of March and continued until the 29$^{\text{th}}$ of April, collecting 5.58×10^{11} electrons on target. We kept an average intensity of 7×10^6 e^-/spill, running three days at 10^7 e^-/spill to study the feasibility of running after LS3 at the highest possible intensities

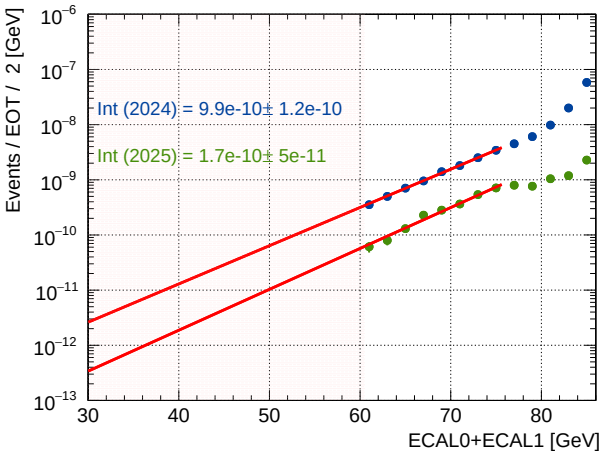

Figure 9. ECAL energy spectra for the 2024 and 2025 runs with corresponding exponential fits, shown at an intermediate selection stage. Events are plotted after applying all selection cuts except the ECAL shower χ^2. Distributions are normalized by the total number of EOT collected in each run.

in the line. As in 2025, similar optics with a narrower beam, improved by G. Dal Masso and N. Charitonidis from CERN BE-EA department, was used. Overall, we had good beam quality, with most of the time 100 units on average on the T2 target and periods with 3 spills per cycle. A summary of the spills accumulated along our run is shown in Fig. 10.

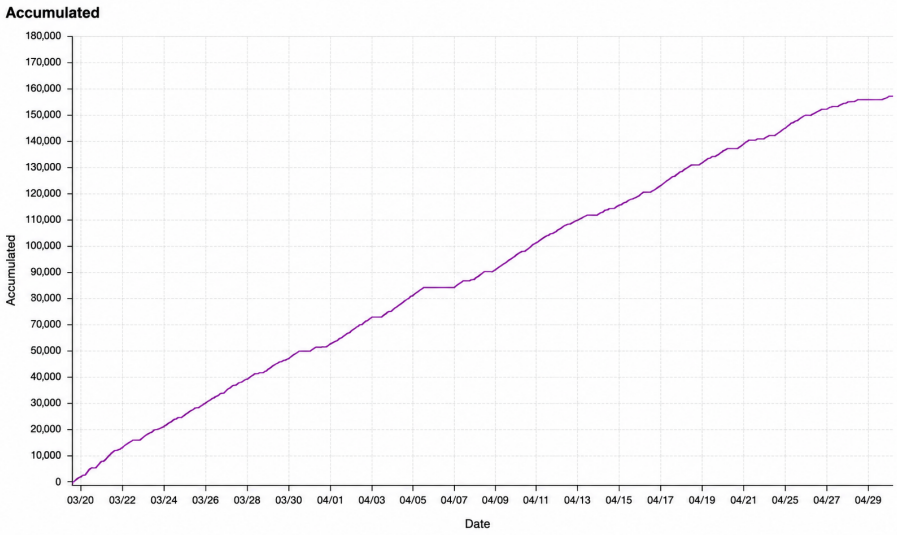

Figure 10. Spills recorded per day during the 2026 run at H4.

During the last five days of the run, a dedicated test was performed to assess the feasibility of a visible A' measurement based on an oriented crystalline target. In 2016 and 2017, NA64 already conducted two dedicated runs to search for a visibly decaying A' exploiting a dedicated setup, with a first compact calorimeter (WCAL) followed downstream by an evacuated decay volume, a set of tracking stations and plastic scintillator

counters, and a second calorimeter (ECAL)[5, 6]. The expected signal due to A' production in the WCAL, followed by its decay to an electron-positron pair in the downstream vacuum vessel, is the observation of events with a low-energy deposition in the WCAL, due to the residual electromagnetic shower developing after A' emission, in coincidence with a high-energy deposition in the ECAL due to the electron-positron pair impinging on it, and with a two-track signal in the tracking stations and plastic scintillator counters. No events within the signal region were observed in the total accumulated sample of about 8.4×10^{10} electrons on target. This result allowed NA64 to set stringent limits on the existence of a visibly decaying A' over a broad range of masses and kinetic-mixing strengths. In particular, at a mass of about 17 MeV, NA64 excluded the kinetic-mixing interval $1.2 \times 10^{-4} < \varepsilon < 6.8 \times 10^{-4}$.

This mass region is of particular interest in connection with the so-called "X17 anomaly". While the X17 hypothesis does not in general correspond to a kinetically mixed dark photon, the NA64 visible-decay search can also be interpreted in terms of the coupling of a hypothetical X17 boson to electrons. More recently, the X17 hypothesis has been tested by both the MEG II and PADME experiments. MEG II found no significant evidence for X17 production in $^7\mathrm{Li}(p, e^+e^-)^8\mathrm{Be}$ transitions, while PADME observed a modest excess at a mass of about 16.9 MeV, with local and global significances of 2.5σ and approximately 1.8σ, respectively [7, 8]. In the X17 interpretation, these results leave a limited region of parameter space around $\varepsilon \sim 10^{-3}$ to be explored.

As discussed in Ref.[9], the current NA64 experimental setup is not optimized for the exploration of this region, due to the very short X17 decay length associated with the relatively large electron coupling in the remaining parameter space, resulting in the e^+e^- daughters being emitted within the WCAL volume. While the size of the latter can still be optimized, a too compact detector would result in sizable energy leakage for signal events, which would thus not satisfy the aforementioned selection cuts. The innovative approach tested during the 2026 run relies on the use of a compact oriented crystalline target. Thanks to the reduction of the effective radiation length induced by the strong electromagnetic fields in the crystal experienced by the impinging electron, the effective size of the first calorimeter can be significantly reduced while maintaining electromagnetic shower containment[10]. The 2026 test was mostly devoted to a first experimental proof of principle of the new technique in NA64. The yield of events with a hard bremsstrahlung photon emitted in the oriented crystal calorimeter and penetrating through it was measured in the on-axis and off-axis configurations, and the results were compared with Monte Carlo predictions. The data analysis is currently in progress, with preliminary results being very encouraging.

2.2 NA64e^+ at H4 beamline

NA64 has developed an LDM search program based on missing-energy measurements with positron beams, complementary to the main electron-beam effort. The key advantage of the positron-based approach is the enhanced signal yield arising from resonant annihilation of beam positrons with atomic electrons through an s-channel dark photon, $e^+e^- \to A' \to \chi\bar{\chi}$, which can increase the signal rate by approximately two orders of magnitude [11]. Be-

ing the atomic electron almost at rest, the missing energy of the process coincides with the initial positron energy E, connected to the A' mass through the resonant condition $m_{A'} = \sqrt{2m_e E}$. Because positrons continuously lose energy while traversing the thick active target, the process remains resonant over a broad range of energies, allowing efficient coverage of the dark-photon mass interval $\sqrt{2m_e E^{\rm thr}_{\rm miss}} < m_{A'} < \sqrt{2m_e E_0}$, where E_0 is the primary beam energy and $E^{\rm thr}_{\rm miss}$ is the missing-energy threshold, typically chosen as a fixed fraction of E_0. By performing dedicated e^+ runs at different beam energies, NA64 can efficiently "scan" the A' mass interval in the $m_{A'} \approx 200$ MeV region, exploiting the wide range of beam momenta available at the H4 beamline. To probe the new technique, NA64 successfully completed two pilot runs, accumulating $\approx 10^{10}$ particles at 100 GeV/c ($\approx 1.6 \times 10^{10}$ particles at 70 GeV/c) in 2022 (2023), exploiting the same setup employed for the main electron-beam program. Despite the limited accumulated statistics, the null observations from the two measurements allowed us to extend the current LDM exclusion limits, covering a new portion of the corresponding parameter space. Results have been published respectively as a letter in PRD (100 GeV/c dataset) [12] and as a more comprehensive JHEP article (70 GeV/c dataset) [13] - details about the two analyses have been reported in previous NA64 yearly reports.

2.3 NA64 hadron

2.3.1 First proof-of-concept K^0_S, K^0_L results

NA64 in hadrons mode (NA64h), utilizing pion, kaon, and proton beams at the CERN SPS, is capable of detecting signals of BSM physics via hadron-nuclear scattering (see Fig. 1). It employs the missing energy technique and some of its specific signatures [14]. NA64h can explore a variety of sub-GeV DM models interacting with the SM via light mediators. Since the dominant production and detection modes for DM occur via hadronic nuclear scattering reactions, NA64h has unique sensitivity to leptophobic (or hadrophilic) DM models with a mediator coupled predominantly to light quarks. These models could yield the correct thermal relic abundance and are difficult to test with NA64e and NA64μ experiments.

NA64h plans to perform a comprehensive study of leptophobic models predicting:

(i) a new $U'(1)$ gauge boson or scalars coupled to LDM [15, 16]

(ii) invisible or semi-visible decays of neutral and vector mesons $\eta, \eta', \omega, \rho^0, ...$ (M^0) [14, 17, 18], and, in particular, $K_{S,L} \to invisible$ decays of neutral kaons, which have never been probed [14, 19, 20]. The later is highly complementary to searches for $K^{+,0} \to \pi + invisible$ decays.

(iii) $K^0 - K'^0$ oscillations of neutral K^0 into its dark partner, e.g., in the Mirror Matter model [21, 22]. This search is complementary to experiments looking for $n - n'$ oscillations at PSI, ILL Grenoble, and SNS ORNL.

(iv) a class of dark sector models with a heavy neutral lepton [23] can also be tested.

In 2024, we published in Physical Review Letter the first results from a proof-of-concept search for dark sectors via invisible decays of pseudoscalar η and η' mesons [24].

Our novel technique uses the charge-exchange (CEX) reaction of 50 GeV π^- on nuclei of an active target as the source of neutral mesons. The $\eta, \eta' \to invisible$ events would exhibit themselves via a striking signature - the complete disappearance of the incoming beam energy in the detector. No evidence for such events has been found with 2.9×10^9 pions on target accumulated during one day of data taking. This allows us to set a stringent limit on the branching ratio $\mathrm{Br}(\eta' \to invisible) < 2.1 \times 10^{-4}$, improving the current bound by a factor of $\simeq 3$. We also set a limit on $\mathrm{Br}(\eta \to invisible) < 1.1 \times 10^{-4}$ comparable to the existing one. These results demonstrate the great potential of our approach and provide clear guidance on how to enhance and extend the sensitivity for dark sector physics for future searches for invisible neutral meson decays [18].

2.3.2 CEX cross sections and results from 2025 run

In 2025 we took another run at H4 with the detector specifically designed to search not only invisible decays of M^0, but also for the first time the $K^0 - K^0_m$ transitions. The experiment employs, the 50 GeV hadron beam with typical beam intensity of the order of $\simeq 10^6$ π^- and $\simeq 3 \times 10^5$ K^- for one SPS spill with 10^{12} protons on target. About 9.48×10^9 particles on target were accumulated during the 2.5 days of the run.

The setup is schematically shown in Fig. 11 was constructed by taking into account lessons from the proof-of-concept run in 2022. The beam of incident charged kaons is defined by the scintillating counters $\mathrm{S}_{1,2,3}$. The momentum of the beam is additionally selected with a momentum spectrometer consisting of a dipole magnet and a low-density tracker, made of a set of Micromegas chambers MM_{1-4}. The η, η', K^0s are produced by beam pions or kaons in charge-exchange reaction $\pi^-(K^-)+(A,Z) \to \pi^0, \eta, \eta'(\bar{K}^0)+(A, Z-1)$ in the scattering off nuclei (A, Z) of the active target (MP). The MP consists of two MiniPoker ($\mathrm{MP}_{0,1}$) PbWO ECAL each of them being a matrix of 3×3 cells of $15 \times 15 \times 200$ mm^3 surrounded by the veto system consisting of a high-efficiency scintillating-Cu veto hadronic calorimeter (VHCAL_1) used against photons or charged secondaries that could escape the target at a large angle. The VHCAL_1 module is also used to form a decay volume DV of the length $L \simeq 0.5$ m for development of the $K^0 - K^0_m$ oscillations. In addition, the VHCAL_1 module and four massive hadronic calorimeter module (HCAL_{0-3}) located at the end of the setup are used as a fully hermetic calorimeter system to detect energy deposited by secondaries from the primary interactions $\pi^-, (K^-)A \to$ anything of $\pi^-(K^-)$s with nuclei A in the target. For searches described in this work, Cherenkov counters ($\mathrm{C}_{1,2}$) are used to identify the incoming kaons and to enhance their tagging efficiency. The veto counter V_2 was used to suppress events with charged secondaries and, importantly, background of backward muons from the $K^- \to \mu^- \nu$ decays in flight upstream of the MP target.

Since there is currently no data available on the values of the cross-sections for the production of light mesons in the CEX reactions with pion and kaon on heavy nuclei, such as W and Pb, the theory group of the Collaboration has made significant efforts to develop phenomenology and calculate these cross sections. This work was recently completed [25], and has been submitted for publication. Briefly, unified description of the CEX reactions (including pion and extending to kaon beams) at wide region of the P_{Lab} from 5 to 200

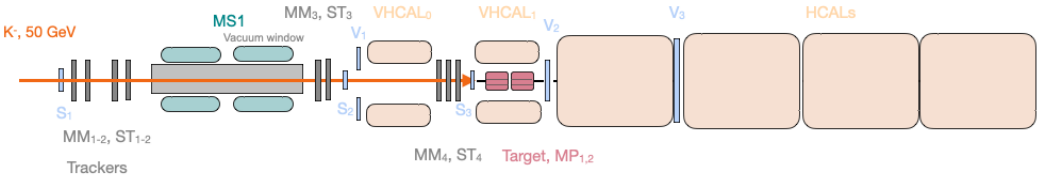

Figure 11. Schematic illustration of the NA64 setup to search for the $K^0 \to K^0_m$ transitions in flight (see text). Here, $\mathrm{MP}_{0,1}$ are denote MP0 and MP1, respectively, throughout the paper.

GeV/c with high-quality fit of existing data (the errors less than 10%) was developed. It is based on the Regge formalism [26–28] and the idea that the corresponding cross section scales as $\left(\frac{s}{s_0}\right)^{2\alpha-2}$, where α is the intercept of the Regge trajectory, s is the total energy squared and $s_0 = 10$ GeV^2 is its initial value. Further details can be found in Ref. [18, 25]. In particular, a generic expression for the integral cross section of the CEX reaction is parametrized by two parameters σ_0 and α as

$$\sigma(s) = \sigma_0 \left(\frac{s}{s_0}\right)^{2\alpha-2}. \tag{2.2}$$

The parameters $\sigma_0 = \sigma(s_0)$ and α are fitted from data.

Our predictions for the the integral cross section of the CEX reactions [25] $\pi^- + p \to \pi^0 + n$, $\pi^- + p \to \eta[\to 2\gamma] + n$, $\pi^- + p \to \eta'[\to 2\gamma] + n$, and $K^- + p \to \bar{K}^0 + n$ read

$$\begin{aligned}
\sigma^{\pi^-}_H(s) &= (109 \pm 13) \left(\frac{s}{s_0}\right)^{2\alpha_\pi - 2} \mu\mathrm{b}\,, \\
\sigma^{\eta}_H(s) &= (29 \pm 2) \left(\frac{s}{s_0}\right)^{2\alpha_\eta - 2} \mu\mathrm{b}\,, \\
\sigma^{\eta'}_H(s) &= (1.05 \pm 0.10) \left(\frac{s}{s_0}\right)^{2\alpha_{\eta'} - 2} \mu\mathrm{b}\,, \\
\sigma^{\bar{K}^0}_H(s) &= (145 \pm 25) \left(\frac{s}{s_0}\right)^{2\alpha_K - 2} \mu\mathrm{b}\,,
\end{aligned} \tag{2.3}$$

where

$$\alpha_\pi = 0.405, \qquad \alpha_\eta = 0.260, \qquad \alpha_{\eta'} = 0.200, \qquad \alpha_{K^0} = 0.248\,. \tag{2.4}$$

As an example, in Fig. 12 we show our predictions for the integral cross sections of the CEX reactions at different nuclei and for $P_{\mathrm{Lab}} = 40$ GeV.

It should be emphasized, that the CEX cross sections shown in Fig. 12 have also been compared with the cross sections obtained using the empirical parameterization given by the expression $\sigma_{CEX}(A, Z) \sim k \cdot Z^{2/3}$ and showed a good agreement within a few %.

In the analysis of 2025 data performed in 2025-26 we searched for dark sectors via invisible decays of pseudoscalar η and η' mesons and also $K^0 - K'^0$ oscillations of neutral kaons into the dark sector. In Fig. 13 the measured distribution of the total energy deposited

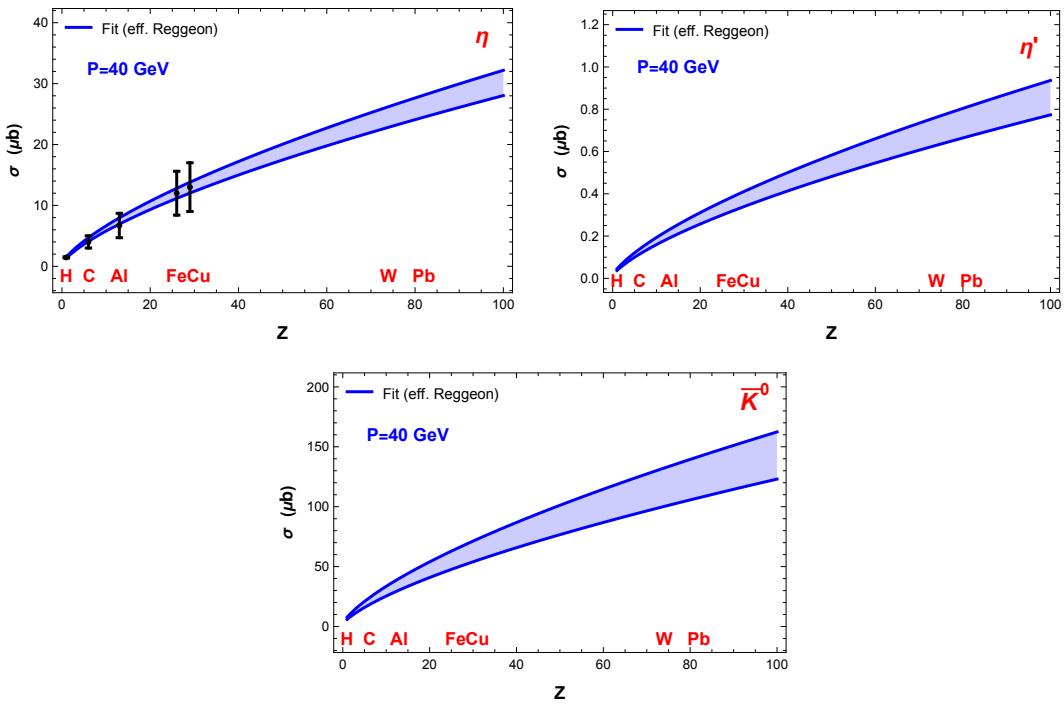

Figure 12. Integral cross section of the CEX reactions with η, η', K^0 production at different nuclei targets and for the values of the $P_{\rm Lab} = 40$ Ge. The dots are from available measurements of CEX η production.

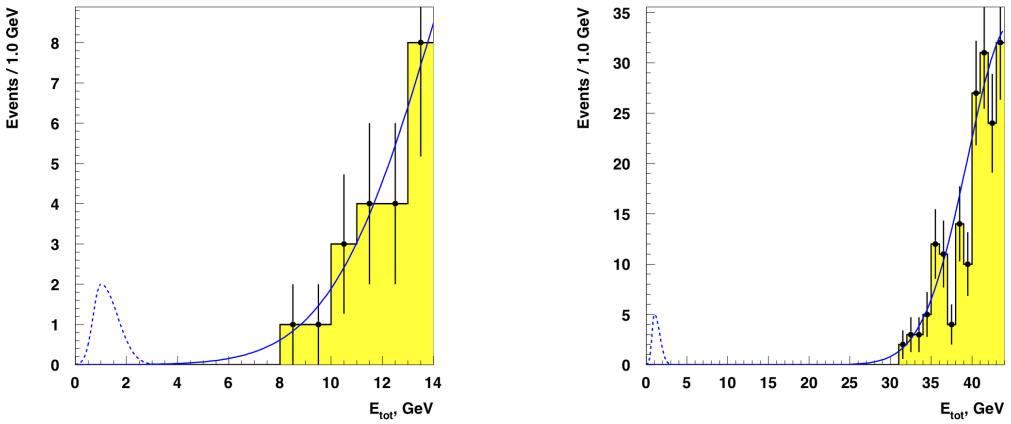

Figure 13. The measured distribution of the total energy deposited in three calorimetry modules (VHCAL1+HCAL0+HCAL1) with signal selection cuts applied, Left panel: events accumulated with 50 GeV pions, Right panel: kaon events. The expected total background contributions (solid black) are overlaid on the data (points) from the shaded area. The shape of the expected signal distribution from the $\eta \to invisible$ decay (dashed blue) is normalized to a few signal events. For the η', K_S, $K_L \to invisible$ the signal shape is very similar.

in calorimetry modules (VHCAL1+HCAL0+HCAL1) for events accumulated with pions (left panel) and kaons (right panel) that passed the signal selection criteria, are shown.

The preliminary analysis indicates no evidence for events with the total missing energy. This allows us to set new preliminary limits on the branching ratio $\mathrm{Br}(\eta \to invisible) < 2.9 \times 10^{-5}$, $\mathrm{Br}(\eta' \to invisible) < 5.8 \times 10^{-5}$, improving our previous bounds by a factor of $\simeq 3$. We also set for the first time the bound on the probability of $K_S - K_{Sm}$, $K_L - K_{Lm}$ oscillations, $P(K_{S(L)} - K_{S(L)m}) < 3.8 \times 10^{-3}$ allowing us to obtain the first limit on the mixing parameter $|\delta\lambda_{S,L}| \lesssim 5.2 \times 10^{-15}$ GeV. This value is close to the limit set by cosmological considerations, and it needs to be improved by an order of magnitude to exceed this bound [22].

The results obtained demonstrate significant potential of our approach using the new setup, and provide a clear guidance on how to enhance and extend the NA64 capability for searching for dark sector physics with invisible neutral meson decays and neutral kaon oscillations after LS3 period.

2.4 NA64μ at M2 beamline

The first search of Dark sectors using the M2 high-energy muon beam was performed with the data collected in 2022 corresponding to 1.98×10^{10} muons on target [29]. These results demonstrated the feasibility of the missing momentum technique. In 2023 and 2024, we collected about twenty times more data ($\sim 3.5 \times 10^{11}$ MOT) than 2022 with a significantly improved setup and an average intensity of $5.6 \times 10^6 \mu$/spill (two times higher than in 2022). The setup is illustrated in Fig. 14. One of the goals was to reduce the main background source identified in 2022 data set [29, 30], the mis-reconstruction of the muon momentum and improve the overall efficiency. A magnet spectrometer, MS1, was introduced upstream of the ECAL interaction point, reducing the 80 meters long level-arm associated with the Beam Momentum Station (BMS) region to $\sim$ 6 meters. The MS1 location was also optimized to further suppress kaon in-flight decays to muons, $K \to \mu + X$, (the second largest source of background) by an order of magnitude, due to the reduced distance between the incoming momentum p_{in}) measurement point and the target. The number of trackers was also increased to 23: 11 MMs (eight 8×8 cm^2 and three 25×8 cm^2), 4 GEMs, and 8 straw stations (two 120×60 cm^2 and six 20×20 cm^2). In addition, the trigger system was improved, including an additional scintillator counter, S_2 in the sketch, to have a better muon telescope and select the beam core. A veto counter, BK, was placed next to S_4 to remove the remaining part of the undeflected beam allowing us to reach intensities a factor of two higher than in 2022. The final trigger was $S_0 \times \bar{V_0} \times S_1 \times S_2 \times S_4 \times \bar{BK} \times S_\mu$. The position of the trigger counters S_4 and S_μ determines the trigger rate and the detectable momentum range of the scattered muon. Finally, the addition of a second prototype VHCAL in the experimental set-up reduces the level of non-hermeticity of the detectors, due to a better rejection of events from upstream interactions with large-angle scattered secondaries.

A blinded analysis of the 2023/2024 data has been performed for the different trigger samples recorded. The signal region is defined by requiring the outgoing muon to have lost at least half of its initial momentum and the total energy deposited in the calorimeters to be compatible with that expected from a single MIP. The setup used in the two runs was similar, but further improvements were included in 2024 in the spectrometers: additional

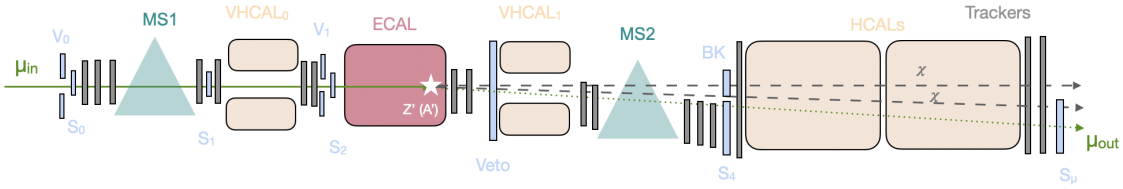

Figure 14. Sketch of the 2023 setup at M2.

and more efficient trackers in the first spectrometer and additional trackers in the downstream one. The 2023 sample has now been unblinded, while the 2024 sample remains blinded. In this report, we present the first results from the unblinded 2023 data together with the status of the blinded 2024 analysis. The following selection criteria were applied:

- *Time selection*: In-time selection in all detectors.
- *a single muon traversing the set-up*: there is only one single track well reconstructed in the upstream and downstream spectrometers (MS1 and MS2). The incoming track has also traversed the scintillator counter in front of the target, S_2.
- *initial muon momentum at 160 GeV*: the momentum reconstructed value is within a $3\sigma_{MS1}$ window.
- *Single hit in the detectors and clean track after MS2*: the tracking detectors located after the ECAL and the MBPL magnet have at most one hit.
- *No energy deposit in the two VHCALs*: an energy below a single-MIP in each VHCAL module.
- *MIP-compatible energy deposit*: in each calorimeter, respectively ECAL and HCAL, the energy deposit below a single MIP. A MIP signal in the central cell of the Veto is also required before VHCAL. In addition, it is verified that the impinging particle crosses the ECAL central cell and that the extrapolated track in the downstream spectrometer matches the energy deposited in the corresponding HCAL cell. These cuts allow the removal of events compatible with muon-nuclear interactions in the target when the ECAL is present.

The hermeticity distributions are shown in Fig. 15 for one representative period of each data sample, after applying the selection criteria described above at different stages. The y axis represents the total energy deposited in the calorimeters, while the x axis corresponds to the momentum of the outgoing muon after the interaction in the target (p_{MS2}). The three panels correspond to different stages of the event selection. The left panels show the distribution obtained by requiring only a muon with existing reconstructed momentum in the MS2 spectrometer. Several regions can be identified in this plot:

(A) Region of MIP-compatible events where $p_{in} \approx p_{out} \approx 160\,\mathrm{GeV/c}$ with the muons traversing the full setup and not been deflected in MS2 with an energy corresponding

to that of a single MIP, $E_{\mathrm{CAL}} < 12\,\mathrm{GeV}$. The reason why these events pass is due to the spatial spread of the beam and the geometric acceptance of the physics trigger ($S_0 \times \bar{V_0} \times S_1 \times S_2 \times S_4 \times B\bar{K} \times S_\mu$).

(B) This region is dominated by muon interactions alone which can also result in neutral particle emission measured in ECAL and/or HCAL.

(C) The events correspond to muon interacting in the HCAL modules.

(D) This region is populated by muon interactions occurring in the ECAL target. Due to the limited size of the HCAL calorimeters and its placement, not energy is fully reconstructed in the HCAL. These events are suppressed after the selection in the Veto calorimeter.

(E) This region showcases events that originate from pile-up. Here two or more muons traversed the entire setup, where the energy of the in-time muon that passed the physics trigger is measured, but the track of a muon outside the time window that only passed counters before the target is reconstructed.

In addition, selecting the momentum reconstructed in MS1 within 3σ of the initial 160 GeV momentum reconstructed reduces the tails of the distribution, as visible in the central panels. This highlights the importance of the upstream spectrometer for accurately reconstruct the incoming muon before its interaction in the target. After applying the full selection criteria, only events consistent with muons traversing the entire setup with momentum $\sim$ 160 GeV and energy deposition compatible with that of a a single MIP survive. The background is extrapolated from the momentum axis side-band from these samples. Fig. 16 illustrates the distributions for a representative sample from 2023 and 2024 data indicating the compatibility among the samples and the understanding of the tails of the distribution. The background level obtained is two order of magnitude lower than the one obtained in 2022.

In this report, we summarise the completion of the 2023 sample analysis. All other possible background sources have been scrutinized including: non-hermeticity in the calorimeters, M2 hadron contamination, muon decays, production of QED di-muon in muon interaction with the target as well as pile-up. For the 2023 collected sample corresponding to 1.2×10^{11} the total background expected in the signal region is < 0.01 .

The improvement in the overall efficiency was also evaluated using the calibration sample (selection of incoming 160 GeV muons using the coincidence of the beam counters in front of the target). After applying all selection criteria, we obtain a fourfold increase in efficiency. Combined with the twofold increase in beam intensity achieved during the 2023/2024 runs, this corresponds to an expected overall enhancement of the total yield by nearly a factor of eight. Further enhancement is expected in 2024 due to the improvement in the tracking system described above. The 2024 analysis is close to completion and we plan to finalise it in the coming month.

After unblinding the 2023 sample no events compatible with a $Z' \rightarrow$ invisible decay charged under $U(1)_{L_\mu - L\tau}$ were observed. This model is used as benchmark model to

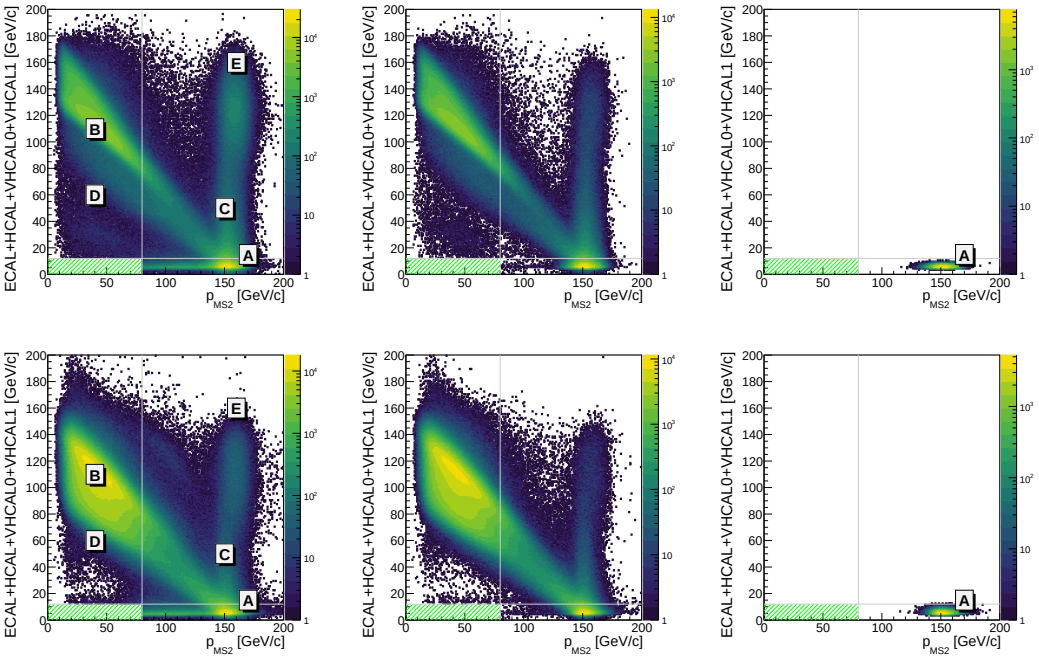

Figure 15. Sum of the energy in the calorimeters versus the momentum of the muon after the interaction in the target for: (*Top:*) The full blinded 2023 period 4 sample in physics trigger corresponding to 7.6×10^{10} MOT. (*Bottom:*) The full blinded 2024 period 3 sample in physics trigger corresponding to 1.92×10^{11} MOT.

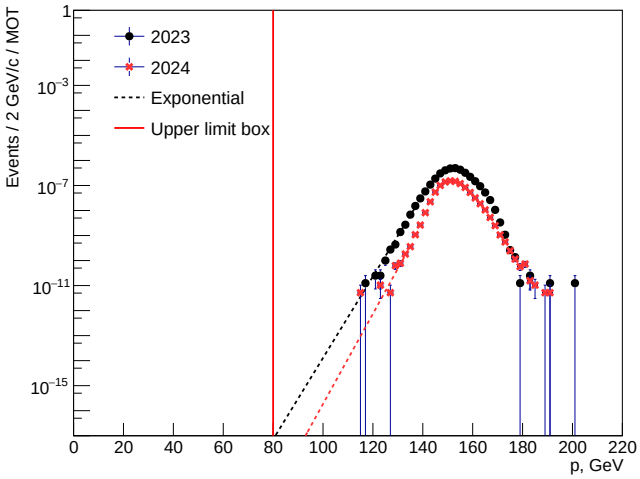

Figure 16. Comparison of extrapolated background from the momentum in MS2 sideband (x axis of 15) using blinded ECAL IN with physics trigger data in 2023 (period 4, 8×10^{10} MOT) and 2024 (period 3, 1.92×10^{11} MOT).

demonstrate the potential of the technique but the search can also be reinterpreted in other models suggesting the existence of a vector-like particle produced in the interaction with the target, as a dark photon. These results allow us to obtain the preliminary 90%

C.L. upper bounds on the coupling of Z' as a function of its mass following the frequentist approach (see Fig. 17). The limits are shown for the minimal scenario considering only decay to neutrinos, the so called vanilla model (left plot) and for extended ones where the Z' can also be a portal to Dark Matter (see the right plot). The green band in the plots shows region compatible to the muon g-2 anomaly. The preliminary results probe all the region below the GeV. In addition, we can cover a significant fraction of the parameter space compatible to the Dark Matter relic prediction in the case of $g_\chi = 5 \times 10^{-2}$.

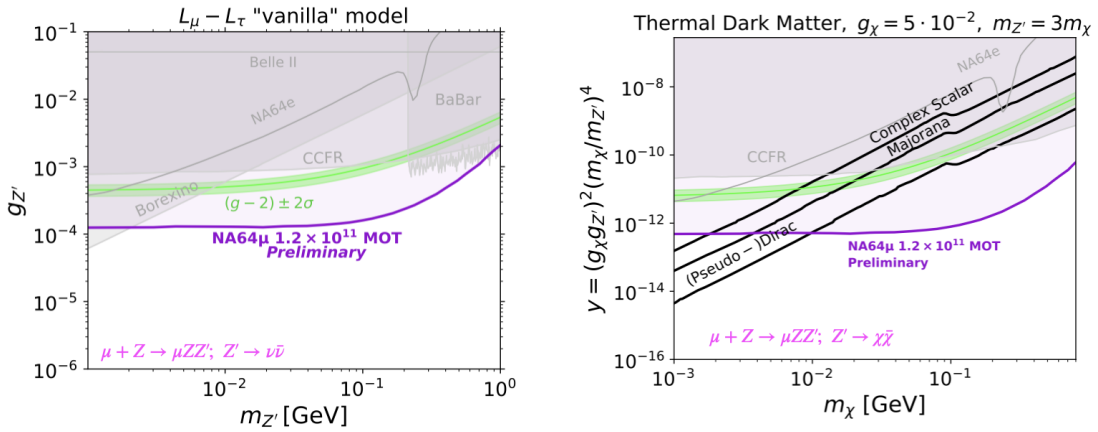

Figure 17. (*Left:*) Preliminary NA64μ 90% C.L. exclusion limits on the coupling $g_{Z'}$ as a function of its mass, $m_{Z'}$, for the vanilla $L_\mu - L_\tau$ model. The two-sigma band for the Z' contribution to muon g-2 discrepancy is also shown. (*Right:*) The preliminary 90% CL exclusion limits obtained by the experiment in the (m_χ, y) parameter space for thermal Dark Matter charged under $U(1)_{L_\mu - L_\tau}$ considering $m_{Z'} = 3m_\chi$ and the coupling $g_\chi = 5 \times 10^{-2}$ for the analysed 1.2×10^{11} MOT. Existing bounds obtained through the CCFR experiment and from other experiments are shown in gray from [30]. See text for details.

3 NA64 plans during LS3 and Run 4

3.1 Planned physics analysis during LS3 period

In this section we describe our plans to exploit the physics potential of NA64 with the data sample collected between 2022 and 2026 runs in the different modes. The increase in intensity and quality of the data recorded during last years will allow us to study Light Dark Matter and other rare processes with unprecedented precision and sensitivity. In the following lines, we provide selected examples of the ongoing activities and the main research directions. This overview is not a complete list.

- NA64e^-: The main goal of NA64e is either to discover or disprove the Light Dark Matter model. The sample collected between 2022 and 2026 correspond to $\sim 3 \times 10^{12}$ EOT. As reported in Sec. 2.1.3 the analysis of the $A' \to$ invisible 2024-2025 data sets is expected to be finished by the end of the year. Next year will be focus on the analysis of 2026 data which did not start as our run finished in May. Besides

the A' purely decaying invisibly hypothesis, the experiment can probe a variety of New Physics scenarios with the 2022-2026 sample as reported in previous sections. In particular we plan to perform the following searches:

- Search for $B-L$ Z' decaying invisibly: The recently published analysis based on the data set up to 2022 provides the most stringent laboratory bounds on the coupling g_{B-L} for sub-GeV masses of the new boson (see Sec. 2.1.1 for further details). Our strategy will be to extend it further for the full data set including 2025-26 data.
- The ALP analysis of the samples collected during 2022 and 2023 has been completed and the analysis on the 2024 data is close to completion. The developed technique for the background rejection will also enable a search for ALPs decaying into photons and into two electrons with the full 2022-26 data sample allowing to extend the sensitivity to the mass range close to the mass of π^0. We also plan to extend the analysis to include semi-visible signatures which can allow us to probe more complex Dark Matter scenarios as inelastic Dark Matter as the ones studied in [31, 32].
- NA64e can also set constrains with the collected data to a generic X boson coupled to electrons, which could be a scalar (S), pseudoscalar (P), vector (V), or an axial vector (A). The available data is 10 times larger than the one used in our first search [33]. In addition, accounting for the resonant annihilation channel with the positrons produced in the electromagnetic shower will enhance the sensitivity at higher masses. These results can also further improve the precision for the comparison of the electron $g-2$ value with the theoretical one, an ongoing experimental effort.
- Searching for Lepton-Flavour Violation in $e^-N \to \mu^- N\phi$ transitions: A magnet spectrometer at the end of the setup was introduced during 2023/2024 runs (see Fig. 8) enabling to probe models involving LFV conversion processes. The NA64 feasibility to carry out these searches was studied using as benchmark model a scalar mediator as a portal to DM. Such boson ϕ, can be produced after an electron collides with a nuclei via Bremsstrahlung and can decay subsequently to DM particles opening a portal to DM detection. The experimental signature in that case is a single muon track created in the ECAL which traverses the HCALs modules, and leaves large missing energy resulting from the production of this new particle using the downstream spectrometer that we add during 2023-2026 runs [34]. The analysis using the data collected during these years will be developed during the LS3 period.

- NA64e^+: in 2025, NA64e^+ collected 3.2×10^9 e^+OT at 45 GeV beam energy and 6.4×10^9 e^+OT at 40 GeV. The analysis of this dataset is currently in progress, the main goal being to probe the LDM parameter space for A' mass value in the 140 MeV - 200 MeV range, exploiting the e^+e^- resonant annihilation channel. In parallel to this, the analysis of $e^+e^- \to \mu^+\mu^-$ events from the two datasets, collected

respectively just below and just above the 43.15 GeV reaction threshold, will allow to measure atomic motions effects associated to in-flight electron-positron annihilation, comparing the measured event yield with that predicted by Monte Carlo simulations for different electron momentum distributions [35].

- NA64μ: The data sample collected in 2023/2024 corresponds to more than an order of magnitude to the one use for our published results on $L_\mu - L_\tau$ LDM. We plan complete the 2024 analysis and the 2023/2024 publication by the end of the year. This search can also be extended to dark photons improving the sensitivity for masses above 0.1 GeV and for scalar-mediated Dark Matter [30]. The sensitivity of the experiment to ALPs, millicharge particles, inelastic Dark Matter and effective muon interactions [36] is also under study.

  In addition, in 2024 we collected data with different triggers. Besides a muon in the final state, we collected a sample which include high energy deposit in the electromagnetic calorimeter, allowing us to study from data muon nuclear interactions. With the data collected we plan to search for $\mu \to$ invisible.

- NA64h: We already published the proof-of-concept searches for invisible neutral meson decays $\eta \to invisible$ and $\eta^{(\prime)} \to invisible$ using the CEX reactions based on 2022 data set. These by-product searches will be extended to the 2025 data sample where the sensitivity is planned to be improved for the η and η' invisible decay modes due to the larger statistics, $2.3{\times}10^9$ pot in 2022 against $9.48{\times}10^9$ pot in 2025, as discussed in Sec.2.3. This analysis will be completed in 2027 and will be possibly extended to invisible decays of other mesons.

  The NA64h has also collected $\simeq 3 \times 10^8$ KoT in the 2025 run, to search for $K_S - K_S^m$ and $K_L - K_L^m$ oscillations into dark sector for the first-time, using the concept of the missing energy in the setup. The analysis of this data sample is ongoing and planned to be completed in 2027.

3.2 Detector upgrade, tests and measurements during LS3

To fully exploit the physics potential described in the previous sections, NA64 will undergo an upgrade during LS3, aimed at maintaining background-free operation at the higher SPS beam rates. Preparatory activities for this upgrade have been supported through the activities performed during 2025 and 2026 runs. The improvements will primarily focused on enhancing the detector hermeticity and the particle identification capabilities, while ensuring efficient data taking at the highest beam rates. The analysis of the large data sets collected before LS3 will also be crucial for defining and optimizing the planned upgrades. The main upgrades currently under development or foreseen during LS3 for the different programs are:

3.2.1 NA64$e^{-/+}$

VHCAL prototype. The outcome of the 2025/2026 analysis would allow us to confirm if the two VHCAL configuration is enough to completely suppress the background from electronuclear interactions.

Radiation hardness. Repairing and replacement of the shashlik counters of the ECAL is essential due to the degradation associated to radiation damage. Based on FLUKA simulations the ECAL has accumulated 4 Mrad during these years. In 2026 run, the fibers of the central counters were already replaced allowing us to improve the light yield.

Enhanced particle ID. A new Lyso-based Synchrotron radiation detector was already used during 2025/2026 runs allowing us to improve the particle identification for low signals. A new monitoring system with a blue laser the calorimeters is also under preparation. Longitudinal segmentation of the four HCAL modules is also planned. Each module will be divided into two sections along its depth, each equipped with a new PMT readout system. In 2026 run, the first HCAL was already equipped with new green-extended photomultipliers to increase the light yield.

Trackers upgrade: new Micromegas and read-out. For the 2026 run, six new Micromegas detectors were built for NA64, with the main upgrade being an optimized design with un-multiplexed readout. The previous generation of NA64 Micromegas used a multiplexing factor of 5 between strips and readout channels. Removing this multiplexing entirely gives unambiguous hit reconstruction, better performance at high occupancy, lower noise, and simpler clustering, all of which are key ingredients for high-rate operation with clean multi-hit reconstruction for pile-up handling. In addition, design corrections were made to improve operational stability. In the previous detectors, sparks were observed due to non-uniformity of the amplification gap, which limited the maximum operating voltage for some detectors. Reverting the multiplex readout in the trackers increases the required quantity of front-end electronics. To limit this increase, the active area was reduced from 8×8 cm^2 to 6.4×6.4 cm^2. Since the NA64 electron beam is highly collimated, no significant acceptance or efficiency loss was observed from this reduction. A new set of four ADC/TDC boards (iFADC-iFTDC [37]) was developed to replace the previous, slower and less reproducible readout electronics, aiming primarily at stable operation and faster detector installation and commissioning. Finally, the gas mixture was changed to use the optimized ternary gas mixture also used by ATLAS [38, 39]. Instead of a locally-mixed Ar : CO_2(93:7%), the detectors now use a premixed gas bottle of Ar : CO_2 : i $-$ C_4H_{10} (93:5:2%). The addition of isobutane improves the secondary avalanches quenching, allowing the detector to be run at higher voltage before reaching the spontaneous breakdown limit at which sparking starts.

DAQ upgrade: new digital trigger system: The current NA64 trigger system is entirely based on NIM electronic modules, implementing the coincidence matrix between the plastic scintillator counters and the electromagnetic calorimeter signals, as well as handling the "begin-of-spill" and 'end-of-spill" signals from SPS and the BUSY signal from DAQ. Although being simple and easy to implement and maintain, the system presents some limitations, namely the limited possibility to reconfigure it and monitor the performances on-line. Also, as discussed in Sec. 2.1.3, the finite width of NIM logic signals introduce a non-negligible inefficiency for the entire system. To circumvent these limitations, we

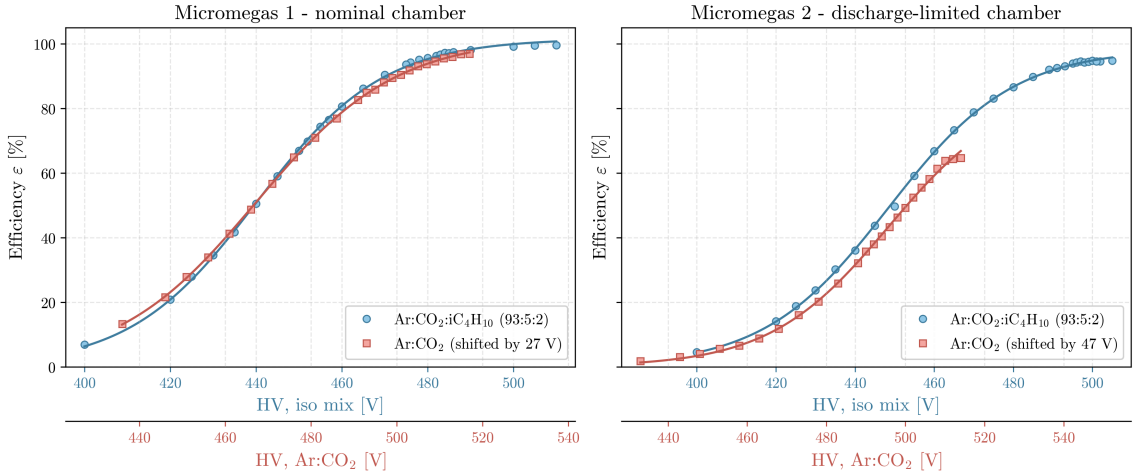

Figure 18. Efficiency vs. high-voltage (HV) for a nominal chamber and a problematic, discharge-limited chamber, comparing Ar:CO_2 (red) with Ar:CO_2 + 2% isobutane (blue). Efficiency is defined as the fraction of events with at least one hit in the chamber. The bottom axis shows the isobutane HV, the axis below it the equivalent Ar:CO_2 HV. In general, isobutane allows operation at ∼30 V lower HV for full efficiency (Micromegas 1). For the discharge-limited chamber, which cannot reach high HV on pure Ar:CO_2 and plateaus around 65% efficiency, isobutane recovers the efficiency to ∼95% at a safe operating voltage.

plan to start a dedicated R&D program devoted to the implementation of a new digital trigger system, based on the digitized signals acquired by the "Waveboard" digitizers for all PMT-based detectors. A PhD student at INFN-Genova, starting Nov. 2026, will be entirely devoted to this effort.

3.2.2 NA64μ

A new zone at M2 beamline is under design in collaboration with the CERN BE-EA department. The 100 m-long region upstream (BMS area) of the experimental setup will be kept under vacuum, thereby minimizing muon interactions along the beamline. In addition, a rail system will be deployed to facilitate changeovers with other M2 users. The support tables for the trigger scintillator counters, tracking stations, and calorimeters will be mounted on rails, allowing the setup to be efficiently moved in and out of the beamline.

The possibility to install the setup slightly downstream is also under study together with D. Banerjee and G. Dal Masso. This will provide a more focused beam, and detailed Monte Carlo simulations are currently being developed to determine the optimal location. The possibility of installing additional tracking or veto detectors near the BMS region is also under investigation, as these could help further suppress the low-energy tail of the M2 beam. We also plan to investigate the possibility to use large-aperture magnets in the MS2 area. We are already discussing this with the CERN BE-EA department and we plan to develop Monte Carlo simulations to determine the optimal parameters.

In terms of detectors we plan to install two other hadronic calorimeters, produce new larger and unmultiplexed Micromegas trackers following the developments for H4. Three new Straw stations of 20×40 cm^2 will also be installed in between the HCAL modules.

In order to cope with higher intensities we plan also to upgrade the trigger and Data Acquisition System to have an independent system at M2. all calorimeters will also be equipped with the new waveboard digitiser readout. Specific funding for such upgrades is going to be requested this year. A preliminary sketch of the setup is illustrated in Fig. 19 indicating also the space of the area needed around.

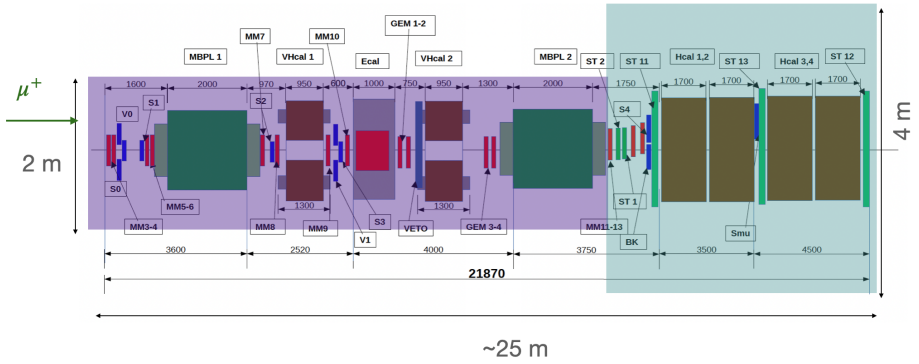

Figure 19. Preliminary sketch of the setup foreseen for post-LS3 runs.

3.2.3 NA64*h*

Veto system: Renew the existing veto system from COMPASS for measuring charge exchange cross sections at PS and SPS.

Target: The major upgrade is foreseen for the target aiming at a significant rejection of background from π^- and K^- decays in-flight. The target is planned to be constructed of two independent sections. The first part will serve to identify the MIP. It will have a hodoscopic structure similar to the MP0 detector shown in Fig.11 but with the total length of $\sim 4-5\ X_0$. The second part, the target itself, is a longitudinally segmented shashlik ECAL module of $\sim 1.5\ \lambda_{int}$ composed of $10-20$ cells, each of which has an individual photo-readout.

3.3 Physics goals for Run 4 and measurements foreseen at PS/SPS during LS3

To fully exploit its physics potential during Run 4, NA64 will undergo an upgrade during LS3 to continue running in background-free mode, guaranteeing stable operation at the higher SPS beam rates as outlined in previous section. A summary document describing the potential of our search using complementary beams and our goals for Run 4 was submitted as input to the ESPP2025 [40], together with the dedicated to the NA64 scientific program submitted to SPSC for the muon[41] and positron [42] programs. A document describing our goals for the hadron program will be submitted next year.

The statistics expected to be accumulated during Run 4, corresponding to $\sim 10^{13}$ electrons, $\sim 10^{11}$ positrons (at 40 and 60 GeV), and $\sim 2\times10^{13}$ muons on target, will allow NA64 to explore new LDM parameter space and many other well-motivated dark-sector

models, with the potential to discover or conclusively test thermal LDM scenarios. In Fig. 20, the NA64 projected sensitivities for Light Dark Matter mediated by a Dark Photon are shown for the two benchmark parameters $\alpha_D = 0.1$ (left plots) and $\alpha_D = 0.5$ (right plots). In the bottom plots, we highlight the combined positron run reach at 40 and 60 GeV as well as the possibility to include a measurement at 150 GeV. Using complementary beams and the Run 4 statistics will allow NA64 to continue leading LDM searches. As described in the report this data would also allow to set competitive limits in many other well-motivated scenarios below the electroweak scale.

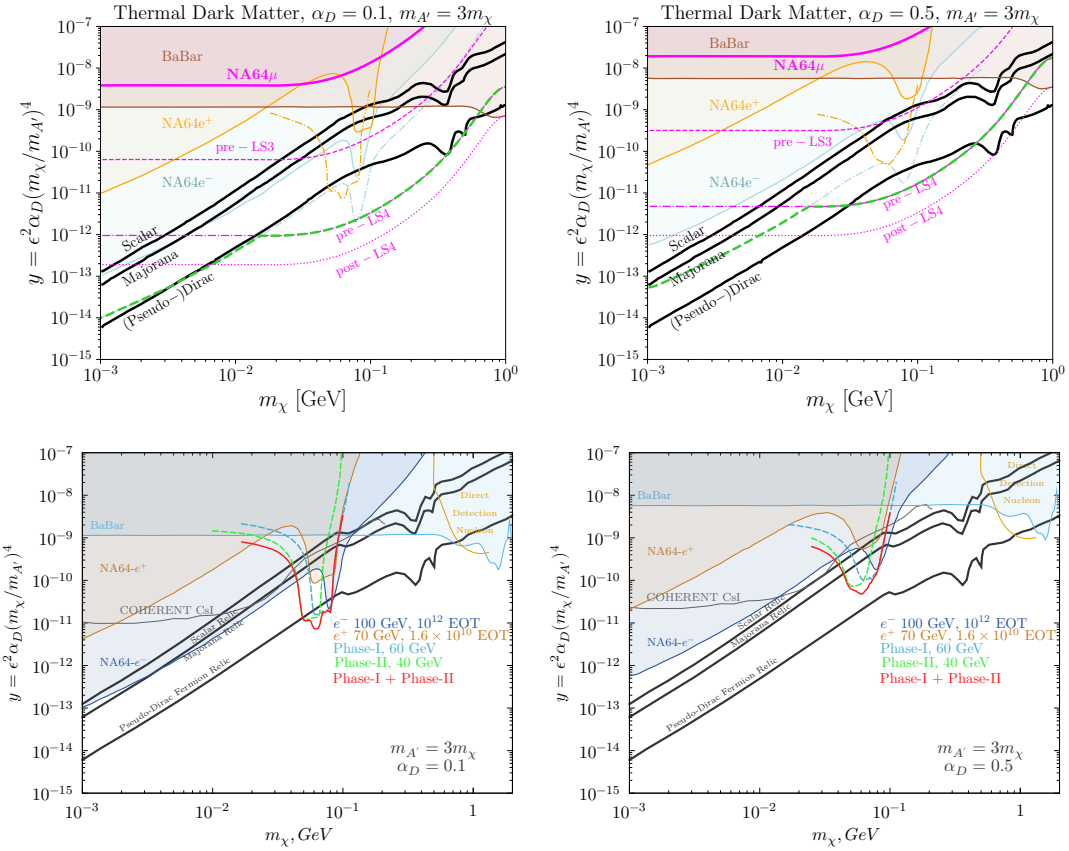

Figure 20. *(Top:) Combined NA64 projected limits for Light Dark Matter mediated by a Dark Photon using the statistics collected during Run 4 with the different programs for $\alpha_D = 0.1$ (left) and $\alpha_D = 0.5$ (right). (Bottom:) NA64 projections for the positron-beam program. The cyan and green curves are the results expected from the 60 GeV and 40 GeV measurement, respectively, while the red curve correspond to their combination. The other curves and shaded areas report existing limits in the same parameters space from NA64 in electron-beam [1] and positron-beam mode [13], COHERENT [43], and BaBar [44]. The black lines show the favored parameter combinations for the observed dark matter relic density for different variations of the model.*

3.3.1 Plan of measurements at PS during LS3

Based on our experience during 2025 and 2026 runs we will exploit the possibility of requesting beamtime at CERN PS T9 beamline to prepare such upgrades and optimise the

foreseen runs at SPS after LS3. Some measurements planned are:

- *Detector tests and caracterisation:* NA64e calorimeter tests and their new laser monitoring system. Tests of new Straw chambers and Micromegas. Tests of the additional HCAL modules for M2. New DAQ and trigger systems tests for electron and muon programs.

- *Dedicated measurements for the hadron program:* In order to enhance the capability of NA64h, we are currently considering the possibility of performing a program of measurements at the CERN PS T9 beamline during the shutdown period LS3. Depending on the final PS schedule, we foresee 3-4 weeks at PS in 2028 to test the new detectors, measure the trigger rate and study the feasibility to measure charge exchange cross-section accurately. In 2029, 4-5 weeks will be requested for CEX cross-section measurements on heavy nuclei with pion and kaon beams in the energy range between 5-15 GeV for comparison with our calculations. We would also like to probe the developed technique of searching for dark sectors using hadron beams at H4 at lower energies as the ones available at the PS. Finally, the possibility of performing a search for $K_L - K_{Lm}$ oscillations at the PS IRRAD facility is also under consideration.

3.3.2 Plan of measurements at SPS after LS3

After the LS3 period we plan to continue collecting data at H4 with the upgraded setups. An overview of the details of the foreseen runs is illustrated in Tab. 1 using the latest schedule available in [45]. Should the SPS restart in 2029 for a shorter running period, we plan to accommodate a three-week commissioning run in the H4 and M2 beam lines. This plan will be adapted once the final SPS schedule is available. Based on our experience during the 2022-2026 run we are requesting a maximum of 10 weeks in H4 to include the time for installation, commissioning and calibration. The positron and hadron runs are scheduled after the electron run to minimise the time for installation and commissioning. At M2 we foresee runs of 8 weeks and they can be accommodated along the SPS year to be better coordinated among the different users. The proposed measurements represent the minimum number of weeks required to achieve our goals for Run 4, but they can be distributed differently across the years to ensure the optimal sharing of the beam lines.

4 Summary

In this report, we have presented the latest results from the NA64 programme, which exploits the missing-energy and missing-momentum techniques with electron, positron, muon and hadron beams available at the CERN SPS. A summary of the physics programme, the statistics collected so far and the main milestones for the post-LS3 phase is presented in Tab. 2. The potential of NA64 to explore dark sectors after LS3 was also presented as input to the European Particle Physics Strategy Update 2025 [40].

In addition to producing new physics results, the 2025 and 2026 runs have provided important input for the definition of the next phase of the experiment, demonstrating that

Program	Beam line	Intensity	Weeks					Run 4 statistics	Accumulated statistics
			2029	2030	2031	2032	2033		
Electron	H4	1.4×10^7	2	8	6	6	6	0.82×10^{12}	1.1×10^{13}
Positron	H4	–	0	3	4	3	3	10^{11}	40, 60, 150 GeV
Muon	M2	$2 \times 10^7, 4 \times 10^7, 20 \times 10^7$	3	8	8	8	0	$10^{13}, 6 \times 10^{13}$	–
Hadron	H4	–	0	0	2	2	2	–	–

Table 1. Summary of the expected data taking periods at SPS during Run 4 for the four programs. We are considering 3500 spills per day based on our current experience. The intensity is the one measured in our beam counters. The statistics is provided as particles on target. In the case of the muon program different intensities are quoted being the gray lines the expected one if the upgrade is totally funded.

the main experimental challenges associated with higher statistics and beam intensities can be addressed. The main achievements and prospects of the different programmes can be summarized as follows:

- e^-/e^+ *programme at H4*: Latest results have been shown on the parameter space of a Z' charged under $U(1)_{B-L}$ models obtained using the full electron-beam dataset collected between 2016 and 2022 and the enhancement of the resonant annihilation channel with the positrons of the shower. For the unbroken, the new limits exceed those from dedicated neutrino-scattering experiments, providing the most stringent laboratory bounds on g_{B-L} for sub-GeV masses of the new boson. In addition, we have done significant progress in the ALP coupled to two photons analysis with the data collected between 2022 and 2026. The 2022-2023 data sets have been unblinded and no signal events have been found compatible with the existence of such particle. The limits obtained using the full 2016-2023 statistics (1.31×10^{12} EOT) set new upper limits on the ALP-photon coupling $g_{a\gamma\gamma}$ for ALP masses up to $m_a \approx 77$ MeV. These results demonstrate the NA64 capabilities of probing a variety of New Physics scenarios beyond Light Dark Matter.

  The electron programme has continued to increase the statistics available for invisible searches, while making substantial progress in the understanding and suppression of the dominant backgrounds. The results obtained with the VHCAL system, together with detailed simulations of electronuclear processes [4], have confirmed the importance of improving the detector hermeticity for the next phase of the experiment. The two-VHCAL configuration deployed in 2025 and 2026 provides an order-of-magnitude suppression of the high-energy tails associated with upstream interactions, in agreement with Monte Carlo expectations. During the 2026 run, 5.6×10^{11} EOT were collected, including dedicated running at 10^7 electrons per spill to test operation at the intensities foreseen after LS3.

  In parallel, significant progress has been made in detector and DAQ developments required for high-intensity operation, including faster waveform digitisation, improved

pile-up reconstruction and rejection, new unmultiplexed Micromegas trackers, and improved particle-identification detectors. These developments, together with the ongoing analysis of the 2024–2026 data, provide the basis for maintaining nearly background-free operation with a target statistics of about 10^{13} EOT after LS3.

The positron programme has demonstrated the power of resonant e^+e^- annihilation for LDM searches. The 70 GeV data, published in JHEP [13], excluded vector-mediated LDM in the range $165 < m_{A'} < 220$ MeV for ε values down to 2.5×10^{-4} and $\alpha_D = 0.1$, despite a statistics almost two orders of magnitude smaller than that accumulated with electrons. Measurements at 40 and 45 GeV performed in 2025 extended the programme towards a scan of different A' masses and simultaneously provided tests of detector technologies foreseen for future running.

Finally, a dedicated test performed during the last five days of the 2026 run demonstrated the feasibility of using an oriented crystalline target for visible searches in the X17 mass region. Preliminary results are very encouraging and provide the basis for further development of this technique during LS3.

- *Muon programme at M2*: The first NA64 muon search established the feasibility of the missing-momentum technique with 1.98×10^{10} MOT and demonstrated its sensitivity to dark sectors coupled predominantly to the second lepton generation [30]. In 2023 and 2024, the accumulated statistics were increased to 3.5×10^{11} MOT, while major improvements were made to the spectrometer, trigger and reconstruction. In particular, the addition of the MS1 spectrometer close to the target substantially reduced the low-momentum tails caused by mis-reconstruction of the incoming muon momentum, which constituted the dominant background in the first analysis.

  The 2023 sample has now been unblinded, corresponding to 1.2×10^{11} MOT, and no events compatible with the signal hypothesis were observed. The resulting preliminary limits significantly improve on the first NA64μ result and probe new parameter space of the $L_\mu - L_\tau$ model, including regions relevant for the muon $g-2$ anomaly and thermal LDM. The 2024 sample remains blinded and its analysis is ongoing. The improvements in reconstruction and selection efficiency, together with the increased beam intensity, result in an expected overall signal yield almost a factor of eight higher than in the first search. The experience gained before LS3 is guiding the design of the upgraded M2 setup, with the long-term goal of accumulating about 2×10^{13} MOT during Run 4.

- *Hadron programme*: The proof-of-concept measurements with hadron beams have established the feasibility of extending the NA64 missing-energy approach to searches for dark sectors coupled predominantly to quarks. The first results based on the 2022 pion data provided limits on invisible decays of η and η' mesons produced through charge-exchange reactions. In 2025, the accumulated pion statistics were increased to 9.5×10^9 POT, allowing these searches to be extended and providing data for the study of charge exchange reactions with pion and kaon beams. In addition, about

Beamline	Particle	Motivation	Latest results	Total stat. pre-2025	2025	2026	Run 4
H4	$\mathbf{e^-}$	*Leptophilic Dark Sectors coupled to e^-:* LDM, inelastic DM, ALPs, scalar, Z', X17	9.37×10^{11}	2×10^{12}	5.9×10^{11}	6×10^{11}	10^{13}
	$\mathbf{e^+}$	*LDM in the $\approx$ 100 MeV mass range via resonance scan*	**100 GeV:** 10^{10} **70 GeV:** 1.6×10^{10}	70 GeV: 2.2×10^{10}	**45 GeV:** 3.24×10^{9} **40 GeV:** 6.39×10^{9}	Oriented crystal test	$>10^{11}$ for different energies
M2	μ	*Leptophilic DS coupled to μ: LDM at masses $\gtrsim$ 100 MeV, ALPs, Z', muon $g-2$, millicharge, $\mu\to\tau$ ...*	1.98×10^{10}	3.5×10^{11}			2×10^{13}
H4/T9	**h**	*Hadrophilic DS; Invisible η, η', K^0 decays*	2.9×10^{9}		9.5×10^{9}	Addendum to be prepared during LS3	

Table 2. Overview of NA64 physics program highlighting its physics goals, the current statistics and our milestones after LS3.

3×10^8 kaons on target were collected to perform the first search for $K^0-K^0_m$ oscillations into the dark sector.

The ongoing analyses, together with the phenomenological description of CEX cross sections developed by the Collaboration, provide the basis for a dedicated hadron programme after LS3. Measurements at the PS during LS3 are foreseen to characterize the available pion and kaon beams, test the upgraded detectors and perform precision measurements of CEX cross sections on proton and nuclear targets. An addendum describing the full hadron programme and its physics reach is in preparation.

These results demonstrate the complementarity of the NA64 electron, positron, muon and hadron programmes and provide a clear path towards the larger statistics foreseen during Run 4. With approximately 10^{13} electrons, 10^{11} positrons and 2×10^{13} muons on target, together with the developing hadron programme, NA64 will be able probe most of the remaining parameter space for canonical thermal LDM scenarios and a broad range of other well-motivated dark-sector scenarios. In this document, we have also summarised our plans to achieve successfully such milestones and our preliminary data taking plans at PS and SPS after LS3.

5 Publications

The collaboration has published the following results since the last report submitted in September 2025:

(i) Y. M. Andreev *et al.* [NA64], "High efficiency veto hadron calorimeter in the NA64 experiment at CERN," Nucl. Instrum. Meth. A **1081** (2026), 170830 doi:10.1016/j.nima.2025.170830 [arXiv:2503.11275 [hep-ex]].

(ii) Y. M. Andreev *et al.* [NA64], "Improved limits on a new Z' in $B-L$ scenarios with the NA64 experiment at CERN," [arXiv:2606.17320 [hep-ex]].

In addition, NA64 members and, in particular, the theory working group of the Collaboration, have contributed with the following publications related to NA64e and NA64$_\mu$:

1. P. Crivelli, J. Hernandez-Garcia, J. Lopez-Pavon, V. M. Lozano and L. Molina Bueno, "First bounds on effective muon interactions using the NA64μ experiment at CERN," JHEP **07** (2026), 31 doi:10.1007/JHEP07(2026)031 [arXiv:2511.11801 [hep-ph]].

2. S. N. Gninenko, S. Kuleshov, V. E. Lyubovitskij, A. S. Zhevlakov, "Charge-exchange reactions with pion and kaon beams in the NA64h experiment at CERN" e-Print:2607.28299 [hep-ph]

3. S. N. Gninenko, N. V. Krasnikov, I. V. Voronchikhin, D. V. Kirpichnikov, "Missing energy signatures of inelastic magnetic dipole DM at NA64e" Phys. Rev. D **113** (2026) 11, 115055; arXiv:2603.28278 [hep-ph].

4. S. N. Gninenko, N. V. Krasnikov, S. Kuleshov, V. E. Lyubovitskij, A. S. Zhevlakov, " Constraints on dark axion portal: Missing energy and fermion EDMs", Phys. Rev. D **113** (2026) 9, 095028, arXiv:2602.11405 [hep-ph].

5. S. N. Gninenko, S. Kuleshov, V. E. Lyubovitskij, P. Crivelli *et al.*, "Probing millicharged particles with NA64μ and LDMX", Eur. Phys. J. C **86** (2026) 2, 140, arXiv: 2505.04295 [hep-ph].

The collaboration has also contributed to several International Conferences and topical Workshops such as: Light Dark World 2025, ICHEP2026, iDM2026, QUARKS2026... where the latest NA64 physics results and the future prospects were presented.

References

[1] Y. M. Andreev et al. *Phys. Rev. Lett.* 131, 161801 (2023). doi:10.1103/PhysRevLett.131.161801.

[2] Y. M. Andreev et al. (2026).

[3] A. Berlin, et al. *Phys. Rev. D* 99, 075001 (2019). doi:10.1103/PhysRevD.99.075001.

[4] Y. M. Andreev et al. *Nucl. Instrum. Meth. A* 1081, 170830 (2026). doi:10.1016/j.nima.2025.170830.

[5] D. Banerjee et al. *Phys. Rev. Lett.* 120, 231802 (2018). doi:10.1103/PhysRevLett.120.231802.

[6] D. Banerjee et al. *Phys. Rev. D* 101, 071101 (2020). doi:10.1103/PhysRevD.101.071101.

[7] K. Afanaciev et al. *Eur. Phys. J. C* 85, 763 (2025). doi:10.1140/epjc/s10052-025-14345-0.

[8] F. Bossi et al. *JHEP* 11, 007 (2025). doi:10.1007/JHEP11(2025)007.

[9] E. Depero et al. *Eur. Phys. J. C* 80, 1159 (2020). doi:10.1140/epjc/s10052-020-08725-x.

[10] M. Soldani et al. *Eur. Phys. J. C* 85, 1239 (2025). doi:10.1140/epjc/s10052-025-14967-4.

[11] L. Marsicano, et al. *Phys. Rev. D* 98, 015031 (2018). doi:10.1103/PhysRevD.98.015031.

[12] Y. M. Andreev et al. *Phys. Rev. D* 109, L031103 (2024). doi:10.1103/PhysRevD.109.L031103.

[13] Y. M. Andreev et al. *JHEP* 06, 256 (2025). doi:10.1007/JHEP06(2025)256.

[14] S. N. Gninenko. *Phys. Rev. D* 91, 015004 (2015). doi:10.1103/PhysRevD.91.015004.

[15] B. McElrath. *Phys. Rev. D* 72, 103508 (2005). doi:10.1103/PhysRevD.72.103508.

[16] B. Batell, et al. *Phys. Rev. D* 100, 095020 (2019). doi:10.1103/PhysRevD.100.095020.

[17] A. S. Zhevlakov, et al. *Phys. Rev. D* 108, 115005 (2023). doi:10.1103/PhysRevD.108.115005.

[18] S. N. Gninenko, et al. *Phys. Rev. D* 109, 075021 (2024). doi:10.1103/PhysRevD.109.075021.

[19] S. N. Gninenko and N. V. Krasnikov. *Phys. Rev. D* 92, 034009 (2015). doi:10.1103/PhysRevD.92.034009.

[20] M. Hostert, K. Kaneta, and M. Pospelov. *Phys. Rev. D* 102, 055016 (2020). doi:10.1103/PhysRevD.102.055016.

[21] S. N. Gninenko, N. V. Krasnikov, and V. A. Matveev. *Natural Sci. Rev.* 1, 5 (2024). doi:10.54546/NaturalSciRev.100105.

[22] S. N. Gninenko and N. V. Krasnikov. *Phys. Rev. D* 111, 115019 (2025). doi:10.1103/btqb-16lt.

[23] B. Bertoni, et al. *JHEP* 04, 170 (2015). doi:10.1007/JHEP04(2015)170.

[24] Y. M. Andreev et al. *Phys. Rev. Lett.* 133, 121803 (2024). doi:10.1103/PhysRevLett.133.121803.

[25] S. N. Gninenko, et al. (2026).

[26] T. Regge. *Nuovo Cim.* 14, 951 (1959). doi:10.1007/BF02728177.

[27] V. N. Gribov. *Sov. Phys. JETP* 26, 414 (1968).

[28] P. D. B. Collins. *An Introduction to Regge Theory and High Energy Physics*. Cambridge University Press (1977). doi:10.1017/9781009403269.

[29] Y. M. Andreev et al. *Phys. Rev. Lett.* 132, 211803 (2024). doi:10.1103/PhysRevLett.132.211803.

[30] Y. M. Andreev et al. *Phys. Rev. D* 110, 112015 (2024). doi:10.1103/PhysRevD.110.112015.

[31] C. Cazzaniga et al. *Eur. Phys. J. C* 81, 959 (2021). doi:10.1140/epjc/s10052-021-09705-5.

[32] M. Mongillo, et al. *Eur. Phys. J. C* 83, 391 (2023). doi:10.1140/epjc/s10052-023-11536-5.

[33] Y. M. Andreev et al. *Phys. Rev. Lett.* 126, 211802 (2021). doi:10.1103/PhysRevLett.126.211802.

[34] A. Ponten, et al. (2024).

[35] F. Arias-Aragón, G. G. di Cortona, and E. Nardi. *JHEP* 10, 174 (2025). doi:10.1007/JHEP10(2025)174.

[36] P. Crivelli, et al. *JHEP* 07, 31 (2026). doi:10.1007/JHEP07(2026)031.

[37] I. Konorov, et al. *JINST* 21, C04020 (2026). doi:10.1088/1748-0221/21/04/C04020.

[38] F. Vogel. *PoS* EPS-HEP2021, 757 (2022). doi:10.22323/1.398.0757.

[39] V. D'Amico et al. *Nucl. Instrum. Meth. A* 1083, 171137 (2026). doi:10.1016/j.nima.2025.171137.

[40] Y. M. Andreev et al. (2025).

[41] D. Banerjee *et al.* [NA64 Collaboration]. Proposal for an experiment to search for dark sector particles weakly coupled to muon at the CERN SPS, CERN-SPSC 2019-002/ SPSC-P-359 (2019).

[42] P. Bisio, et al. Light dark matter search with positron beams at NA64. Technical report, CERN, Geneva (2024).

[43] D. Akimov et al. *Phys. Rev. Lett.* 130, 051803 (2023). doi:10.1103/PhysRevLett.130.051803.

[44] J. P. Lees et al. *Phys. Rev. Lett.* 119, 131804 (2017). doi:10.1103/PhysRevLett.119.131804.

[45] CERN. Long-term schedule for the cern accelerator complex. https://edms.cern.ch/ui/file/2311633/6.0/ACC-PM-MS-0004_6_0.pdf (2026).